 Bull. Chem. Soc. Jpn., 75, 641–659 (2002)

Accounts

Gel Formation Analyses by Dynamic Light Scattering

Mitsuhiro Shibayama* **and Tomohisa Norisuye†**

Neutron Scattering Laboratory, Institute for Solid State Physics, The University of Tokyo, Tokai, Ibaraki 319-1106

†Department of Polymer Science and Engineering, Kyoto Institute of Technology, Matsugasaki, Sakyo-ku, Kyoto 606-8585

(Received August 14, 2001)

A novel methodology for non-destructive and real-time determination of the gelation threshold for both chemical and physical systems has been proposed. This method i.e., a *time-resolved dynamic light scattering* (TRDLS) measurement, allows one not only to determine the gelation threshold but also to investigate critical dynamics near gelation threshold, mechanism of gelation, and architecture of gelling cluster. The gelation threshold was found to be characterized by (1) the appearance of a speckle pattern in the scattering intensity, (2) a power-law in the intensity–time correlation function (ICF), (3) a specific broadening of the distribution function, and (4) a noticeable suppression of the initial amplitude of ICF. All of these features originate from some unique aspects of gels: *nonergodicity, frozen inhomogeneities*, and *divergence of connectivity correlation*. As an application of these concepts, we propose four methods for determination of gelation threshold and examine their validity and usefulness for various types of gels; these include chemical gels of *N*-isopropylacrylamide, a gelling system of silica gel in a reaction batch, thermoreversible physical gels of poly(vinyl alcohol)–Congo Red complex, and biological gels of gelatin and globular protein.

Gels have been attractive materials throughout human history. For example, gelatin has been one of the most popular gels over centuries. Everybody has an experience to observe how a soup loses fluidity by cooling. Egg-white, milk protein, extracts from sea-weeds, such as agarose, amylose, and carrageenan, have also been widely used in daily life. All of these materials have been so close to our daily life that we often forget to ask ourselves how it undergoes gelation. A gel is a "bag-free" liquid container in which a large amount of liquid is arrested by a small amount of networking compounds. For example, only a few grams of gelatin powder are necessary to immobilize 100 grams of water. Such kind of gel formation can only be achieved by participation of long-chain molecules or colloid particles having a specific interaction capable of network formation. Recently, gels have been highly developed as a container of liquid, such as water-absorbing materials, chemical reactor and actuators, etc.[1] Now might be a good chance to revisit this intriguing problem, i.e., gelation.

Compared with the long history of gels, scientific studies on gels and on gelation have only a half-century history. This is not an exaggeration if one traces the literature. One of the pioneering works can be found in the paper by Eldridge and Ferry in the 1950s, who proposed a van't Hoff equation for the thermodynamics on the cross-linking process of gelatin.[2] Theory of gelation, i.e., sol-gel transition, of polymers was initiated by Flory in 1940s. He discussed the criterion of infinite cluster formation of polymer chains by polycondensation of two and three-functional monomer mixtures.[3–5] The classical picture of gelation on the basis of Bethe lattice is given by Stockmayer.[6,7] A scaling theory of the gelation was developed by Stauffer,[8] and the critical phenomenon of gelation was discussed by Stauffer et al. on the basis of percolation theory.[9,10]

Among various theories on sol-gel transition, the site-bond percolation theory developed by Coniglio et al.[11,12] is well suited for describing connectivity of monomers at sol-gel transition and phase behavior. A unique but important concept of this theory lies in the participation and its effect of solvent, such as liquid-liquid phase separation in addition to sol–gel transition. Figure 1 shows a schematic illustration of sol–gel transition phase diagram. The ordinate and abscissa denote the bond probability, P_{bond}, and site probability, P_{site}, respectively. The cartoons on the right demonstrate sol–gel transition by P_{bond}, while keeping $P_{\mathrm{site}} = 1$. On the other hand, those on the top show sol–gel transition by P_{site}. P_{bond} and P_{site} of course correspond to the cross-linker concentration and monomer (network constituent) concentration, respectively. It will be shown later that this model is quite suitable for understanding the differences in temperature-induced and concentration-induced sol-gel transitions of reversible gels.

Studies on sol–gel transition are summarized in various reviews and books, such as experimental studies on sol–gel transition of polymers and biopolymers by Guenet,[13] scaling argu-

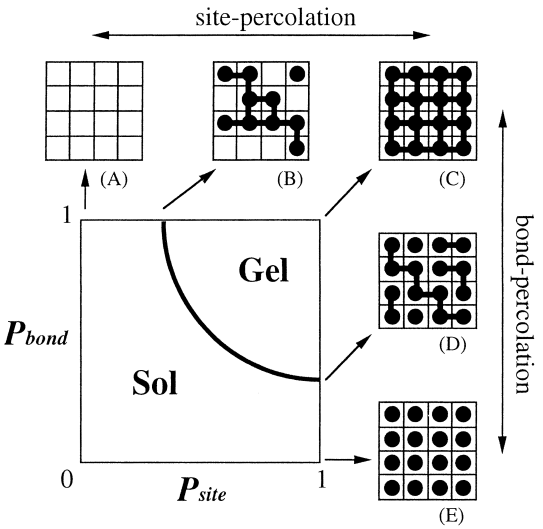

Fig. 1. Sol–gel phase diagram predicted by site-bond percolation theory. The ordinate and abscissa denote bond probability and site probability, respectively.

ments on the static and dynamic properties of branched polymers near the sol-gel transition by Adam and Lairez,[14] reviews on rheology of liquid–solid transition[15] and on thermoreversible network.[16] However, to our knowledge, there are no systematic studies on *real-time and non-destructive gel point determination* in the literature. The objective of this review is to demonstrate a powerful methodology of gel point determination by using dynamic light scattering.

In this review, sol–gel transition will be discussed for various types of gelling systems. Particularly, poly(*N*-isopropylacrylamide) (NIPA) gels cross-linked with *N*,*N*′-methylenebisacrylamide (BIS) will be frequently referred to as a chemical-irreversible gelling system with the abbreviations given above. It should be noted here that NIPA gels were employed not only due to their temperature sensitivity[17] but also to their chemical stability against strong bases and acids.[18] Compared to NIPA gels, polyacrylamide gel, which is more popular in electrophoresis, is easily degraded by ionization and is not suitable for quantitative studies of dynamics if it is prepared by redox polymerization. Gelatin and poly(vinyl alcohol)–ion complex systems will be introduced as examples of physically gelling systems. Heat induced gelation of β-lactogloblin will also be briefly discussed.

It should be noted here that there exist several types of i*nhomogeneities* in gels, which play significant roles to characterize gels and gelation thresholds. However, differences among inhomogeneities and their physical implication have not been extensively discussed so far. Therefore, it is of importance to define here the inhomogeneities for better understanding of gels. The top part of Fig. 2 indicates concentration fluctuations in polymer solutions (left) and in gels (right). In polymer solutions, only thermal concentration fluctuations exist, of which the average is zero. On the other hand, gels contain both frozen concentration fluctuations (the low frequency component in this figure) introduced by cross-linking and thermal concentration fluctuations (high frequency component). The introduction of cross-links brings about various types of inhomogeneities, as shown in the lower cartoons. The *spatial inhomogeneities* are nonrandom spatial variations of cross-link density in a gel, which result in anomalous scattering. The *topological inhomogeneities* represent defects of network, such as dangling chains, loops, chain entrapment, etc. These inhomogeneities affect the dynamics and swelling behavior of gels. Third, the *connectivity inhomogeneities* are dependent on cluster size, distribution, and architecture of polymer chains. It is not an exaggeration to claim that these connectivity inhomogeneities govern the dynamics of the system and become significant at the sol–gel transition threshold as *critical dynamics*. The *mobility inhomogeneities* correspond to variations of local degree of mobility by introduction of cross-links. The mobility inhomogeneities are the reason why scattering speckle appears exclusively in gel state. It is well known that static scattering is useful to study the spatial inhomogeneities and *spatial correlation*. However, as will be shown in this review, dynamic light scattering is superior to static scattering because it allows one to obtain more important information, such as *dynamic correlation* and *connectivity correlation* of polymer chains.

1. Experimental Studies on Sol–Gel Transition

1.1. Conventional Methods of Gel Point Determination. Fluidity (i.e., flow behavior) measurements are the easiest and most handy methods of gel point determination. Those include a tilting-a-tube method and a boll-drop method, which are based on the difference in the flow behavior between sol and gel. The names of these methods themselves explain how they are used. Though these methods are crude, they are widely used to determine gelation threshold.[13,16,19] However, the determination becomes inaccurate for a viscous fluid. The gelation threshold can be accurately determined by viscoelastic measurement. Winter and co-workers[20] proposed a novel method to determine the gelation point with an oscillatory shear experiment. The storage, $G'(\omega)$, and loss moduli, $G''(\omega)$, become equal and scale to ω^u, at the gelation point, i.e.,

$$G'(\omega) = G''(\omega) \sim \omega^u \tag{1}$$

where ω is the angular frequency and u is the viscoelastic exponent. Its validity was examined on the cross-linking process of polydimethylsiloxane[21] and dihydroxypoly(propylene oxide) (model polyurethane)[22] and so on. Today, this method is widely used for quantitative analyses of gelation.[15]

Polymers undergoing gelation via crystallization can be studied by thermal measurements, such as differential scanning calorimetry (DSC). Isotactic polystyrenes in several organic solvents are typical systems studied by DSC.[13,23] NMR is sensitive to the local environment of chemical species of interest. NMR signals become broader and relaxation becomes slower by gelation. An example is found in a ^{13}C NMR work on sol–gel transition of poly(vinyl alcohol) aqueous solution.[24] If a gelation takes place via helix formation, the gel point can be studied by optical rotation measurement. Those include gelation of collagen solution and gelatin gels.[25] In addition to these methods listed above, there are several methods of gel point determination, most of which make use of a drastic change of fluidity.

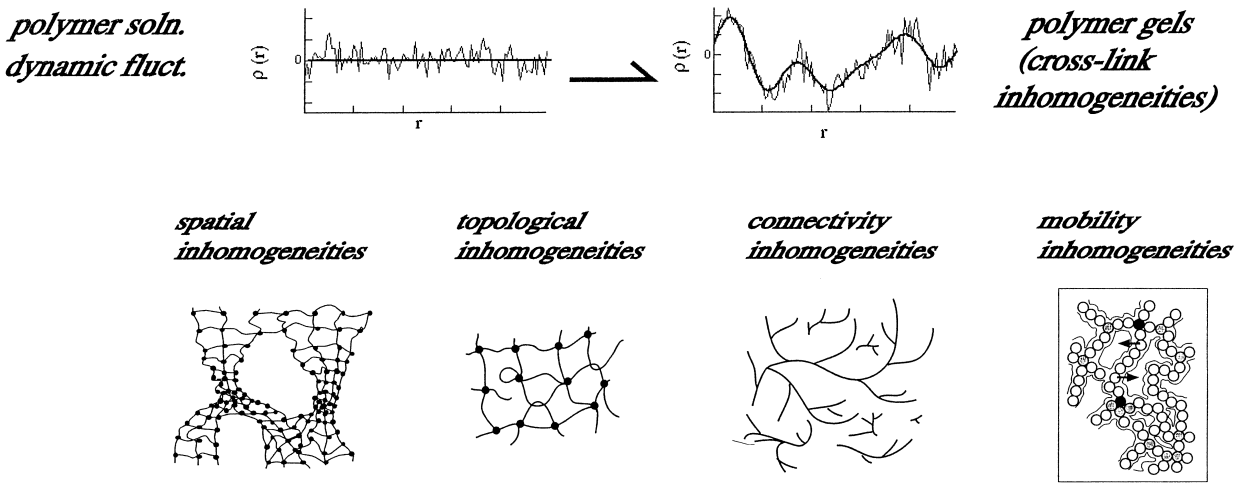

Fig. 2. Inhomogeneities in polymer gels. The upper figures illustrate the difference in concentration fluctuations between polymer solutions (left) and polymer gels (right). For polymer gels, in addition to thermal fluctuations, frozen inhomogeneities are superimposed.

1.2. Sol–Gel Transition Studies by Scattering Methods. Compared with rheological methods, an in-situ (or a real time) determination of the gelation threshold by scattering has been thought to be difficult because of the following reasons. Scattering signals in a gelling solution are dominated by interference between different clusters evolving by gelation. This interference conceals structural information on individual clusters. Hence, in order to investigate *spatial correlation* of concentration fluctuations, a scattering study has to be carried out on a diluted system. Experimental studies on sol–gel transition by light scattering,[26,27] small-angle X-ray scattering,[28] and small-angle neutron scattering[29] were conducted by terminating gelation reaction, followed by dilution so as to observe single cluster scattering.

Only a few studies were carried out on a reaction bath without dilution. Kobayashi[30] introduced a method which uses speckles to detect the gelation point of a gelatin solution. He studied a mixture of gelatin with polystyrene latex spheres in water by static light scattering. The sample test tube was rotated during the experiment. When the sample reached the onset of gelation, strong speckles appeared. Speckles are dots of light scattered or reflected by a sample as non-zero cancellations of concentration (or density) fluctuations.[31] Allain et al.[32] used a similar method to detect the onset of gelation of acrylamide. Again, polystyrene micro-beads of submicrometer size were dispersed in the pregel solution. In both cases, it was assumed that polystyrene micro-beads are allowed to move freely if the mesh size of the medium is much larger than the size of the micro-beads, giving rise to a low scattered intensity. However, by gelation the system reaches the point at which the mesh size is reduced to become comparable to that of the micro-beads. At this point, the movement of micro-beads is frozen, resulting in a strong scattering as a speckle pattern. Wu et al.[33] also showed that speckles are a useful measure for an in-situ detection of infinite network formation in epoxy resin. However, the physical implication of speckles was not extensively discussed. In the following section, let us briefly review the theoretical background of light scattering and dynamic light scattering.

2. Theoretical Background of Light Scattering and Dynamic Light Scattering

2.1. Static Light Scattering Light scattering is one of the standard tools for characterization of polymer solutions. The measure is the scattering vector (or momentum transfer) defined by $q = |\mathbf{q}| = (4\pi n_0/\lambda)\sin(\theta/2)$, where λ is the wavelength of the light in vacuum, n_0 is the refractive index of the solvent, and θ is the scattering angle. By measuring scattering intensity as a function of q, one can evaluate the structure and shape of the scatterer. The scattering intensity $I(q)$ from a dilute polymer solution is given by[34,35]

$$\frac{KC}{I(q)} = \frac{1}{\langle M\rangle_{\mathrm{W}}}\left[1+\frac{\langle R_g^{\,2}\rangle_{\mathrm{Z}}}{3}q^2\right] + 2A_2C + 3A_3C^2 + \ldots \quad (2)$$

where C is the polymer concentration, A_2 and A_3 are the second and third virial coefficients, respectively, $<M>_{\mathrm{w}}$ is the weight average molecular weight, and $<R_{\mathrm{g}}^{\,2}>_{\mathrm{z}}$ is the z-average-square radius of gyration. K is a constant given by

$$K = \frac{4\pi^2 n_0^2\left(\dfrac{\partial n}{\partial C}\right)_0^2}{N_{\mathrm{A}}\lambda^4} \quad (3)$$

where $(\mathrm{d}n/\mathrm{d}C)$ is the refractive index increment with respect to C, and N_{A} is Avogadro's number. Equation 2 indicates that the scattered intensity at $q = 0$ is proportional to the mass of the polymer and to the concentration at low concentrations, i.e.,

$$I(q=0) \sim C\langle M\rangle_{\mathrm{W}} \quad (4)$$

In the case of finite concentrations, $KC/I(q)$ is usually plotted as a function of q and C. This is the so-called Zimm plot. Infinite dilution is unattainable for a gelling system because the final polymer concentration in a gel must be higher than the chain overlap concentration C^* to form an infinite cluster and chain connectivity prevents infinite dilution. As polymeriza-

tion proceeds, C becomes greater than C^*, interference between molecules screens all of the molecular characteristics, such as $<M>_w$ and $<R_g^2>$ and Eq. 2 is no longer applicable.

For semi-dilute polymer solutions ($C > C^*$), "blob scattering" is observed due to concentration fluctuations in a blob, of which the scattering function is given by

$$I(q) \sim \frac{1}{1+\xi^2 q^2} \tag{5}$$

where ξ is the correlation length.[36] The magnitude of ξ, however, is expected to be a few hundred angstroms at most. Hence, a q-dependent scattering appears in small-angle X-ray or neutron scattering regime instead of in light scattering. Figure 3 shows an example of absolute scattering intensity functions obtained for a NIPA gel and the corresponding poly-NIPA solution obtained by static light scattering (LS) and small-angle neutron scattering (SANS). The contrast factor K for neutron scattering is given elsewhere.[37] These gels and solutions were prepared by redox polymerization at 10 °C with NIPA concentration of $C_{NIPA} = 690$ mM and the cross-linker concentrations of $C_{BIS} = 8.62$ mM (gel) and $C_{BIS} = 0$ mM (solution). Note that this set of concentrations is a typical recipe for electrophoresis. The solid line denotes a fit with Eq. 5. As shown here, ξ is on the order of 10 Å (1 nm) and q dependence of $I(q)$ for the solution is very weak in the LS regime. On the other hand, $I(q)$ of the gel is much stronger than expected by Eq. 5 in both LS and SANS regime. It is clear that the scattering intensity function for gels cannot be represented by a Lorentz function like Eq. 5, and a strong "excess" scattering appears as shown in Fig. 3. This excess scattering is called cross-linking inhomogeneities (related to the spatial inhomogeneities in Fig. 2) and has been an issue of debate for more than a decade, as reviewed in the literature.[38,39]

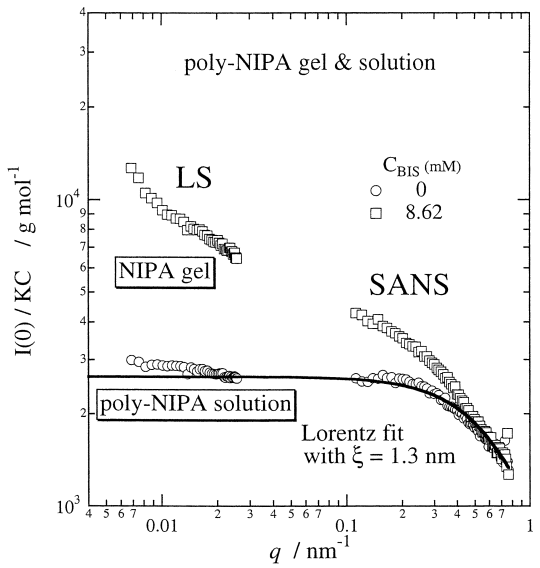

Fig. 3. Example of observed scattering intensity by light scattering (LS) and small-angle neutron scattering (SANS) for NIPA polymer solutions and gels. The data were normalized with the contrast factor K (both for LS and SANS) and concentration C. The solid line is a fit with Eq. 5.

As mentioned above, in the case of static scattering, in principle, it is necessary to quench the polymerization reaction, irrespective of the way of polymerization, e.g., stepwise polymerization, chainwise polymerization, or vulcanization. This process is followed by dilution of the system in order to characterize the cluster size, cluster size distribution. Dynamic light scattering (DLS), on the other hand, does not require such a procedure since it provides information about the dynamics of the system without strong disturbance of interference effects as will be shown later.

2.2. Dynamic Light Scattering. DLS is quite useful to study the dynamics of chain molecules and clustered molecules in a solvent and of gels.[40] It provides information on *translational diffusion* of individual polymer chain clusters as well as on *collective diffusion* (an internal mode of chain dynamics). One of the first reported observations of DLS from gels was given by Prins et al. in 1972.[41] They observed a syneresis in a gelatin gel. In 1973, Tanaka, Hocker, and Benedek (THB) proposed a theory of collective diffusion of polymer network by treating it as a continumm.[42] This became one of the standard methods to describe the dynamics of gels.[43] This theory predicts that intensity correlation function (ICF), $g^{(2)}(t)$, is given by a single exponential function even if cross-links are randomly introduced to a polymer solution. However, the THB theory did not take account of the inhomogeneities present in the gels (See Fig. 2). Since the spatial inhomogeneities act as local oscillators, heterodyne-type analyses were often employed in the late 1970s through the 1980s.[40,44,45] In 1989, Pusey and van Megen proposed a completely different concept, the nonergodicity.[46] This is based on the concept that a gel is a nonergodic medium. In the following, a brief review of theoretical developments on the dynamics of gels is given.

2.2.1. Collective Diffusion of Ergodic Systems. The dynamics of polymer solutions can be investigated by taking the intensity time-correlation function (ICF) as a function of decay time, τ. The intensity time-correlation function (ICF), $g^{(2)}(\tau)$, is given by

$$g^{(2)}(\tau) \equiv g^{(2)}(\tau;q) = \frac{\langle I(0;q)I(\tau;q)\rangle_T}{\langle I(0;q)\rangle_T^2} = \left|g^{(1)}(\tau;q)\right|^2 + 1 \tag{6}$$

where $<I(\tau; q)>_T$ is the scattering intensity at time τ with respect to $\tau = 0$ and the scattering vector q, and $<\ldots>_T$ denotes a time average. $g^{(1)}(\tau)$ is the scattering field time-correlation function given by a Laplace transform of the characteristic decay time distribution function, $G(\Gamma)$, i.e.,

$$g^{(1)}(\tau) = \int_0^\infty G(\Gamma)\exp(-\Gamma\tau)d\Gamma \tag{7}$$

where Γ^{-1} is the characteristic decay time. In the case of semidilute polymer solutions and of gels, $g^{(1)}(\tau)$ can be approximated by a single exponential function, i.e.,[42]

$$g_{T,p}^{(1)}(q,\tau) = \exp(-Dq^2\tau) \tag{8}$$

where D can be either the translational diffusion coefficient or the collective diffusion coefficient dependent on the system, i.e., a dilute polymer solution ($C < C^*$) or semidilute polymer

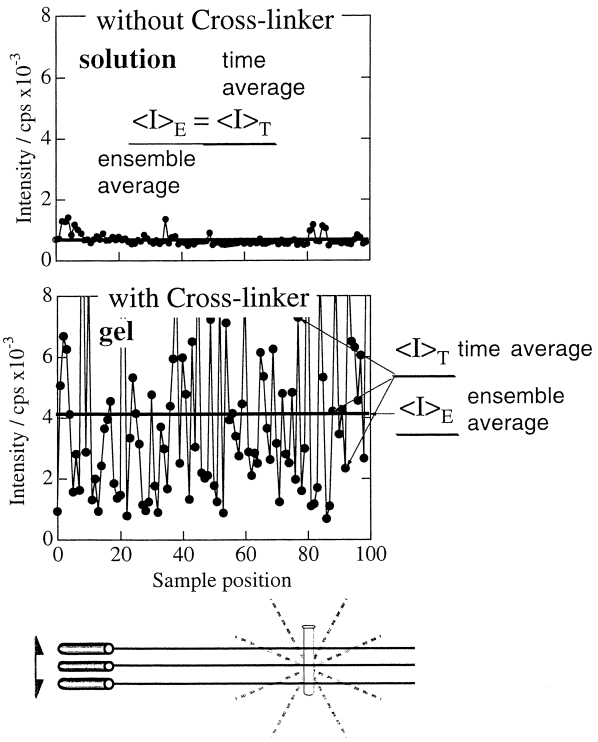

Fig. 4. Comparison of speckle patterns between polymer solution (upper) and polymer gels (lower).

solution ($C > C^*$), respectively. The ICF, however, becomes position dependent when gelation takes place. This is due to the nonergodic nature of gels as pointed out by Pusey and van Megen[46] and by Xue et al.[47]

2.2.2. Speckles and Nonerogidicity. When an infinite network is formed, the polymer chains in the network lose their freedom to travel freely in the phase space and are arrested in a limited phase space. This results in non-cancellation of concentration fluctuations and emergence of position-dependent concentration fluctuations (i.e., frozen inhomogeneities). These types of frozen inhomogeneities are observed as a speckle pattern. Figure 4 shows a comparison of speckles for polymer solution (poly-NIPA solution) and NIPA gels (C_{NIPA} = 690 mM, C_{BIS} = 8.62 mM), where the scattering intensity at $\theta = 90\,^\circ$ was measured by scanning sample positions.[48] Both systems were made from the same concentration of NIPA, while BIS concentrations was C_{BIS} = 0 mM (solution; upper) and 8.62 mM (gel; lower). In the case of the gel, the scattering intensity strongly fluctuates with sample position. Each speckle corresponds to time-average scattering intensity, $<I>_T$. On the other hand, an ensemble-average scattering intensity $<I>_{\mathrm{E}}$ is obtained by taking an average over the sample positions. The inequality, i.e.,

$$\langle I\rangle_{\mathrm{E}} \neq \langle I\rangle_{\mathrm{T}} \tag{9}$$

is one of characteristic features of gels. A system in which the ergodic hypothesis does not hold is called a *nonergodic* system. It is known that glasses and gels are nonergodic systems.[46]

2.2.3. Intensity Correlation Function for Nonergodic Systems. In order to explicitly describe position dependence, let us use an index of position, p, arbitrarily chosen in a gel. Then, $I(\tau; q)$ has to be replaced to $I_p(\tau; q)$ and two types of average scattering intensity are defined, i.e., time $<I_p(\tau; q)>_{\mathrm{T}}$ and ensemble averages $<I(\tau; q)>_{\mathrm{E}}$. The former is dependent on p, whereas the latter is independent of p by its definition,

$$\langle I\rangle_{\mathrm{E}} \equiv \langle I_p(\tau,q)\rangle_{\mathrm{E}} = \frac{1}{N}\sum_{p=1}^{N}\langle I_p(\tau,q)\rangle_{\mathrm{T}} \tag{10}$$

where N is the number of sampling points in a sample. It is needless to mention that $<I>_{\mathrm{E}}$ is not equivalent to $<I_p>_{\mathrm{T}}$ for nonergodic media. Accordingly, time average $g_{\mathrm{T},p}{}^{(2)}(\tau)$ and ensemble average intensity correlation functions $g_{\mathrm{E}}{}^{(2)}(\tau)$ are separately defined by

$$g_{\mathrm{T},p}{}^{(2)}(\tau) = \frac{\langle I_p(0;q)I_p(\tau;q)\rangle_{\mathrm{T}}}{\langle I_p(0;q)\rangle_{\mathrm{T}}^2},$$

$$g_{\mathrm{E}}{}^{(2)}(\tau) = \frac{\langle\langle I_p(0;q)I_p(\tau;q)\rangle_{\mathrm{T}}\rangle_{\mathrm{E}}}{\langle\langle I_p(0;q)\rangle_{\mathrm{T}}^2\rangle_{\mathrm{E}}} \tag{11}$$

Figure 5 illustrates the difference in the two types of averaging for ICF. In the case of polymer solutions, the scattering intensity $<I>_{\mathrm{T}}$ is solely due to thermal concentration fluctuations. Hence, $<I>_{\mathrm{T}} = <I_{\mathrm{F}}>_{\mathrm{T}}$ and no speckles appear, where $<I_{\mathrm{F}}>_{\mathrm{T}}$ is the intensity component due to thermal concentration fluctuations. The intensity correlation function does not depend on how it is averaged. On the other hand, a glass is a frozen system of which concentration fluctuations are totally frozen. This gives rise to a speckle dependent $<I>_{\mathrm{T}}$, i.e., $<I_p>_{\mathrm{T}}$, where no time-fluctuating component exists. In this case, the time average of ICF differs from the ensemble average as shown in the figure, e.g., $g_{\mathrm{T},p}{}^{(2)}(0) = 1$ and $g_{\mathrm{E}}{}^{(2)}(0) = 2$. Note that there is no relaxation in glasses. A gel is in between these two extremes.

Now, let us describe the time-average intensity correlation function, $g_{\mathrm{T},p}{}^{(2)}(\tau)$, for gels. $g_{\mathrm{T},p}{}^{(2)}(\tau)$ can be regarded as consisting of homodyne and heterodyne components, and is given by[49]

$$g_{\mathrm{T},p}{}^{(2)}(q,\tau) = X_p{}^2|g_{\mathrm{T}}{}^{(1)}(q,\tau)|^2 + 2X_p(1-X_p)|g_{\mathrm{T}}{}^{(1)}(q,\tau)| + 1 \tag{12}$$

where X_p is the ratio of the scattering intensity of the fluctuating component to the total intensity at sample position p, i.e.,

$$X_p = \frac{\langle I_{\mathrm{F}}(q)\rangle_{\mathrm{T}}}{\langle I_p(q)\rangle_{\mathrm{T}}} \tag{13}$$

The origins of homodyne and heterodyne scattering are schematically explained in Fig. 6. The incident light is scattered by scattering elements, such as monomers constituting a gel network. If the scattering element is moving around by thermal agitation, the scattering intensity decays with a factor of exp $(-Dq^2\tau)$ (see Eq. 8). This type of relaxation takes place at each scattering element. As a result, the time intensity correlation function (ICF) given by Eq. 6 has the term of exp $(-Dq^2\tau)\times$exp $(-Dq^2\tau)$ = exp $(-2Dq^2\tau)$ (*homodyne scattering*).[50] However, if some of scattering elements lose mobility, it

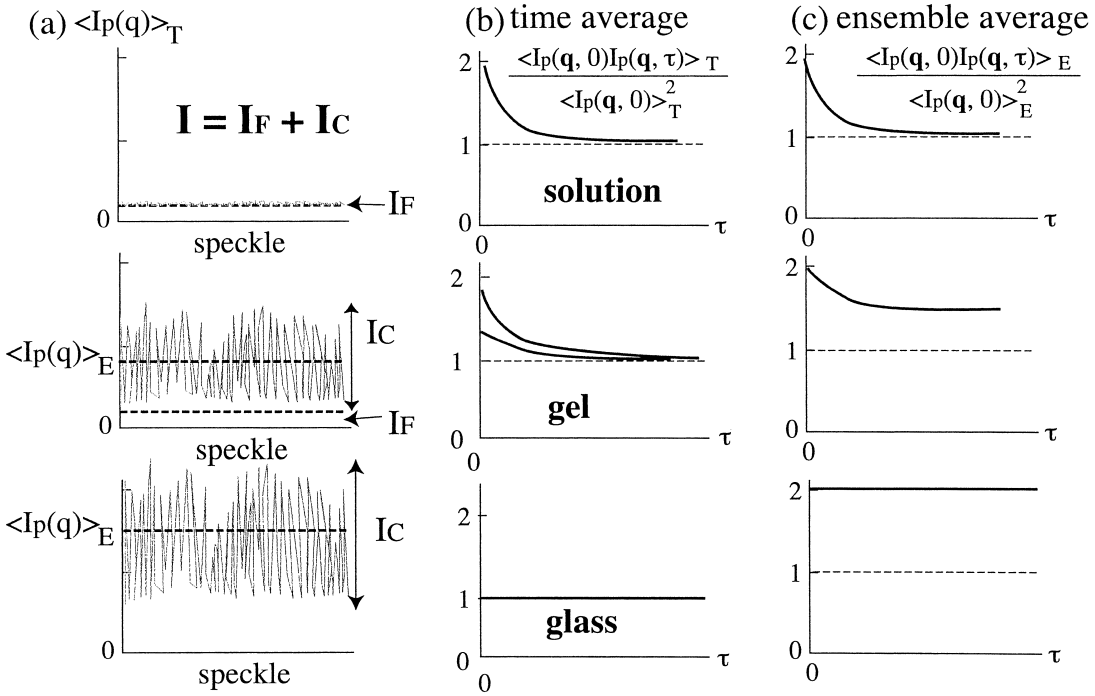

Fig. 5. Illustration of (a) speckles, (b) time-average intensity correlation functions (ICF), $g_{T,p}^{(2)}(\tau)$, and (c) ensemble-average ICF, $g_E^{(2)}(\tau)$, for solutions, gel, and glasses.
[Reproduced with permission from *Physica A*, **157**, 705–730 (1989). Copyright 1989 Elsevier Science]

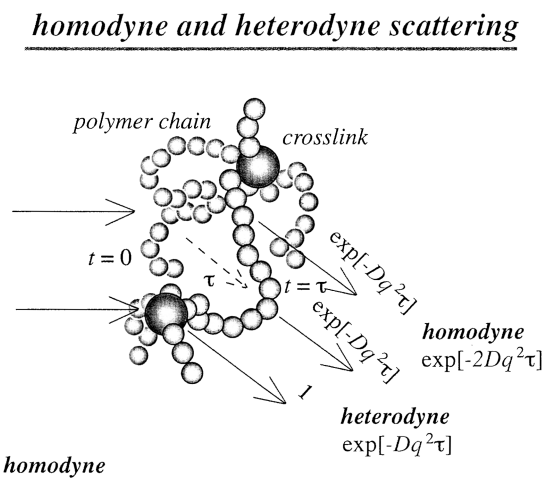

Fig. 6. Schematic illustration explaining homo and heterodyne scattering.

behaves as a local oscillator and the term exp $(-Dq^2\tau)$ becomes unity. Hence, the decay part of ICF becomes $1\times\exp(-Dq^2\tau) = \exp(-Dq^2\tau)$, instead of $\exp(-2Dq^2\tau)$. This is the case of *heterodyne scattering* and is often observed when local oscillators, such as impurities, exist in the system. The crosslinking point may act as a local oscillator, and the resultant ICF contains some portion of heterodyne components. On the basis of this concept, the so-called partial heterodyne method was proposed by Joosten et al.;[49] this allows one to decompose the scattered intensity to two contributions, i.e., scattering from the (liquidlike) dynamic fluctuations and scattering from the (solidlike) spatial inhomogeneity.

2.2.4. Decomposition. The initial slope of $\ln[g_{T,p}^{(2)}(\tau)-1]$ can be approximated by a single exponential function at least for a gel made at $C >> C^*$, from which an apparent diffusion coefficient, $D_{A,p}$, is obtained;

$$D_{A,p} = -\frac{1}{2q^2}\frac{\partial}{\partial\tau}\ln\left[g_{T,p}^{(2)}(\tau)-1\right]_{\tau=0} \tag{14}$$

Note that $D_{A,p}$ is sample position, p, dependent.[46,49] From Eqs. 8, 12, and 13, one obtains

$$D_{A,p} = \frac{D}{2-X_p} \tag{15}$$

where D is the collective diffusion coefficient. Alternatively, D and $\langle I_F\rangle_T$ can be determined by plotting $\langle I\rangle_{T,p}/D_A$ as a function of $\langle I\rangle_{T,p}$ by using the following equation,[39,48,51]

$$\frac{\langle I_p\rangle_{T,p}}{D_{A,p}} = \frac{2}{D}\langle I_p\rangle_{T,p} - \frac{\langle I_F\rangle_T}{D} \tag{16}$$

The collective diffusion coefficient D is related to the spatial correlation function $g(r)$,[52]

$$D = \int\frac{kT}{6\pi\eta r}g(\mathbf{r})d\mathbf{r}\Big/\int g(\mathbf{r})d\mathbf{r} \tag{17}$$

and $g(r)$ is given by[36]

$$g(r) = \frac{\xi}{r}\exp\left(-\frac{r}{\xi}\right) \tag{18}$$

where k is the Boltzmann constant and η is the solvent viscosity. Hence, ξ can be estimated from D,

$$\xi = \frac{kT}{6\pi\eta D} \tag{19}$$

Equation 19 is equivalent to the Stokes–Einstein equation for dispersed systems.

2.2.5. Cluster Distribution Analysis. Equation 7 indicates that the field-correlation function, $g^{(1)}(\tau)$ can be obtained by a Laplace transform of the decay-rate distribution function $G(\Gamma)$. This Laplace transform is given by the following relationship;

$$F(s) = L\{f(t)\} \equiv \int_0^\infty f(t)\exp(-st)dt \tag{20}$$
$$f(t) = L^{-1}\{F(s)\}$$

Therefore, the position dependent distribution function, $G_p(\Gamma)$, can be estimated by the inverse Laplace transform of ${g_{\mathrm{T},p}}^{(1)}(\tau)$,

$$G_P(\Gamma) = L^{-1}\{{g_{\mathrm{T},p}}^{(1)}(\tau)\} \tag{21}$$

or

$$G_p(\Gamma) = L^{-1}\left\{\sqrt{{g_{\mathrm{T},p}}^{(2)}(\tau)-1}\right\} \tag{22}$$

An inverse Laplace transform can be carried out numerically. Among many algorithms, the CONTIN method (the constrained regularization method) is justified to be one of the most faithful methods.[50,53,54] In the following discussion, we often use the decay time distribution function in stead of $G_p(\Gamma)$, where

$$P_p(\Gamma^{-1}) = G_p(\Gamma) \tag{23}$$

This decay time distribution function is quite useful to visualize the cluster-size distribution function of a gelling system since Γ^{-1} is proportional to the cluster size R via Eq. 19, i.e.,

$$R = \frac{kTq^2}{6\pi\eta}\Gamma^{-1} \tag{24}$$

It will be shown that a characteristic broadening occurs in $P_p(\Gamma^{-1})$ exclusively at the gelation threshold.

2.2.6. Asymptotic Behavior of Time-intensity Correlation Function near the Gelation Point. According to the literature,[55] ICFs for sol and gel can be described by the following functions:

$${g_{\mathrm{T}}}^{(2)}(\tau)-1 \approx {\sigma_{\mathrm{I}}}^2\{A\exp(-Dq^2\tau) + (1-A)\exp[-(\tau/\tau_{\mathrm{c}})^{\beta}]\}^2 \text{ (sol)} \tag{25}$$

$${g_{\mathrm{T}}}^{(2)}(\tau)-1 \approx {\sigma_{\mathrm{I}}}^2\{A\exp(-Dq^2\tau) + (1-A)[1+(\tau/\tau^*)]^{(n-1)/2}\}^2 \text{ (gel point)} \tag{26}$$

where ${\sigma_{\mathrm{I}}}^2$ is the initial amplitude of ICF, A is the fraction of the collective diffusion mode, and D is the diffusion coefficient of the fast mode. τ_{c} is the characteristic time for the stretched exponential mode and β ($0 < \beta < 1$) is the stretched exponent. τ^* is the characteristic time where the power law behavior appears and n ($0 < n < 1$) is the fractal dimension of scattered photons. The essential feature of Eqs. 25 and 26 is that the shape of ICF changes drastically from a stretched exponential to power-law behavior at the gelation threshold. Several examples of this type of transition will be given later.

2.2.7. Power-Law Exponent. In the case of viscoelastic exponent, a wide range of u values ($0 < u < 1$) (Eq. 1) are reported in the literature: e.g., 0.5,[22] $n = 0.2 \sim 0.5$,[56] 0.7,[57,58] and its physical meaning is discussed in conjunction with polydispersity and the screening effect of excluded volume.[59] As will be shown later, many gelling systems exhibit a clear power-law behavior in the intensity correlation function at the gelation threshold. Since DLS is sometimes called microrheology, the exponent n is closely related to the viscoelastic exponent, u. Doi and Onuki[60] discussed dynamic coupling between stress and composition in polymer solutions and blends, and obtained

$$n = 1-2u \tag{27}$$

while Adam and Lairez[14] obtained

$$n = u \tag{28}$$

These relations are very controversial. Although the derivation of Eq. 27 seems to be robust, the experimental results rather support Eq. 28.[61,62] This problem does not seem to be settled. Hence, in this article, we simply refer to the values of n for qualitative discussion in this review. In general, the power-law exponent, n, increases with increasing degree of branching.

3. Gel Analyses by Dynamic Light Scattering

3. 1. Time-Resolved Light Scattering. Figure 7 shows scattering intensity $I(t)$ variations during the polymerization process of NIPA branched chain molecules (left) and NIPA linear chain molecules (right) via redox polymerization as a function of reaction time t.[63] The intensity data were taken at every tenth second. The NIPA monomer concentrations at preparation, C_{NIPA}, were increased from 88 mM (top) to 690 mM (bottom). Several important features can be drawn from this simple experiment. (1) $I(t)$ suddenly increases at a threshold time t_{th} (at around 20 min in this particular case). (2) There is a characteristic concentration above which $I(t)$ decreases after passing a maximum. (3) $I(t)$ for the branched chain systems is much larger than that for the linear chain systems, (4) In the case of linear chains (right figures), $I(t)$ is rather stable for $t > t_{\mathrm{th}}$, while $I(t)$ strongly fluctuates with t ($> t_{\mathrm{th}}$). Though all of these phenomena eloquently indicate formation of gels (or polymer chains) at $t \approx t_{\mathrm{th}}$ for the branched chains with $C_{\mathrm{NIPA}} >$ 138 mM, we point out just one aspect in this section.

The abrupt increase and the following decrease in $I(t)$ is explained in Fig. 8. Before $t < t_{\mathrm{th}}$ (stage I), there are no polymer chains. Hence, $I(t)$ is very weak in stage I. However, at $t \approx t_{\mathrm{th}}$ (stage II), polymer chains grow very rapidly with time, resulting in an abrupt increase in $I(t)$. Here, $I(t)$ increases with t since both C (of polymer chains) and $<M>_{\mathrm{w}}$ increase (see Eq. 4). This effect is more evident in the case of branched systems than in that of linear chains; the reason will be discussed later. An independent experiment about the so-called chain overlap concentration (C^*) measurement[63,64] indicated that the determined C^* was roughly the same as the concentration at which

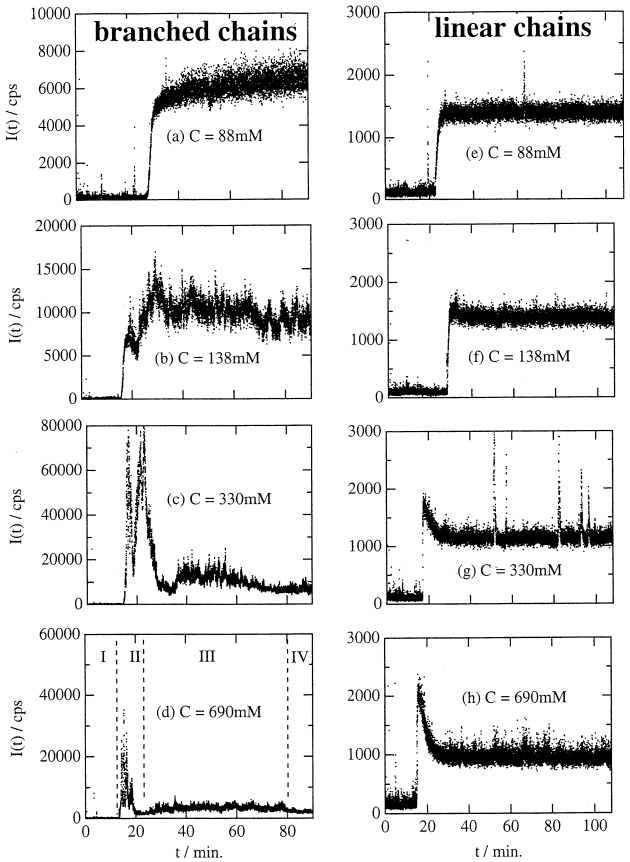

Fig. 7. Scattering intensity variation with time, $I(t)$, during polymerization of NIPA linear (left) and branched chains (right) with various monomer concentrations, Cs.

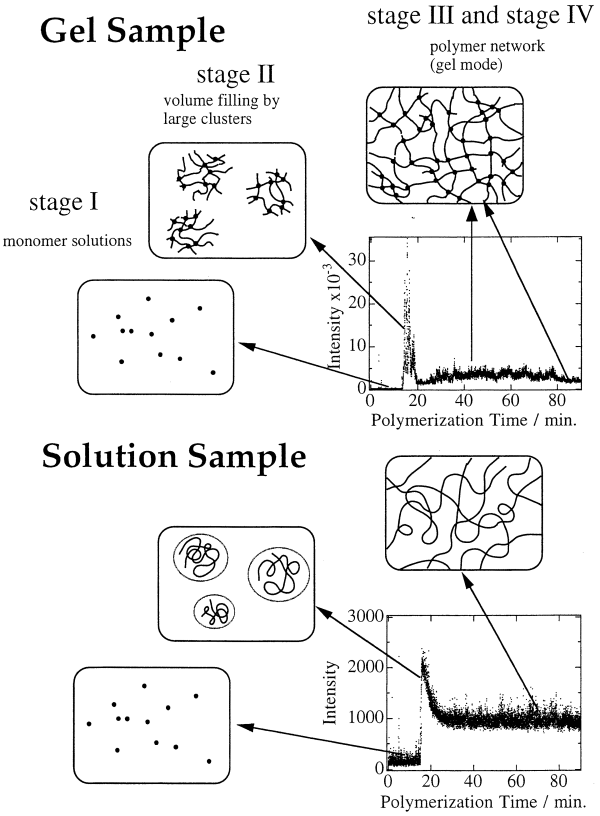

Fig. 8. Schemeatic representation of cluster evolution for gel (branched) and solution (linear) polymer samples. [Reproduced with permission from *Polymer*, **39**, 2769–2775 (1998). Copyright 1998 Elsevier Science]

I_{peak} ($\equiv I(t \approx t_{th})$) deviated from $I_{plateau}$ ($\equiv I(t >> t_{th})$). Hence, it can be concluded that t_{th} is the gelation threshold for the branched systems and the chain overlap threshold for the linear chain systems. In other words, the rapid increase in scattering intensity is an indication of gelation threshold. It will be shown later that this statement is correct for all of the gelling systems studied so far.

It is interesting to note that $I(t)$ of the branched systems with $C = 690$ mM has a pulse-like increase at $t \approx t_{th}$. This phenomenon is analogous to a vapor-to-liquid transition in fluid systems.[65] A monomer solution is a "dispersed" system whose concentration fluctuations are analogous to those of a gas, e.g., carbon dioxide gas. On the other hand, a gel is condensed matter like liquid carbon dioxide. The concentration fluctuations allowed for the system are only those from their averages. At the border between the two phases, a critical opalescence is observed. This corresponds to the pulse-like increase in $I(t)$. Hence, time-resolved light scattering is sensitive enough to detect a gelation threshold.

3. 2. Dynamic Light Scattering from Nonergodic Systems. A systematic study of DLS measurement was carried out for a series of reactor batch poly-NIPA systems prepared with various monomer concentrations, C_{NIPA}, while the cross-linker concentration, C_{BIS} was unchanged ($C_{BIS} = 0$ or 8.62 mM). Figure 9 shows a comparison of the cluster distribution function, $P(\Gamma^{-1})$ for linear polymer chains (prepared without cross-linker) and branched polymer chains in water.[66] Note that five curves of $P(\Gamma^{-1})$ ($\equiv P_p(\Gamma^{-1})$) are shown for each case so as to examine the position dependence of $P(\Gamma^{-1})$ as well. C_{NIPA} was varied from 60 to 690 mM in both cases. In the case of $C_{NIPA} = 60$ mM, there is some difference in the shape of $P(\Gamma^{-1})$ dependent on presence/absence of cross-links, but it is not significant.

When NIPA concentration was increased to $C_{NIPA} = 100$ mM, however, a characteristic broadening in $P(\Gamma^{-1})$ took place exclusively in the branched polymers. This is due to formation of huge clusters owing to the aid of cross-links. This process is analogous to a "merging-and-acquisition" in a stock market, i.e., unification of companies by merging and acquisition. On the other hand, the linear polymer system does not allow such a cluster evolution because of a lack of "binder", and each chain grows simply by addition of a monomer to the growing front of the chain. Interestingly, when C_{NIPA} is further increased, both $P(\Gamma^{-1})$s of the two systems shift to the fast decay time direction and become similar to each other. The shift is puzzling if one considers only translational diffusion of clusters. However, this shift is easily explained with a concept of collective diffusion. For $C_{NIPA} >> 100$ mM, the initial monomer concentration is high enough to form a polymer solution filled in the space. In this case, translational diffusion of individual chains is strongly suppressed (linear polymer chains) or totally annihilated (branched polymer chains) and only local thermal fluctuations between entangled chains (or cross-links)

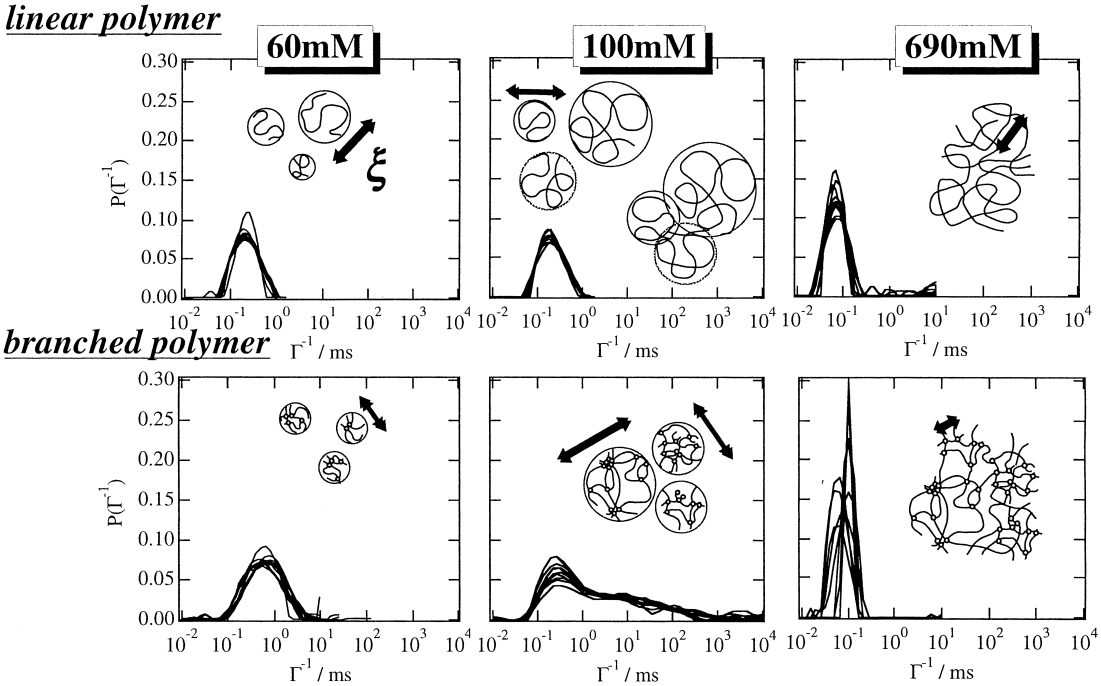

Fig. 9. Characteristic decay time distribution, $P(\Gamma^{-1})$, for linear (upper) and branched NIPA polymer (lower) chains prepared with various monomer concentrations, Cs.

are allowed. This type of fluctuation is observed as a collective diffusion of polymer chains and it is hard to distinguish between linear and branched chain cases for $C > C^*$ except by the position dependence of each $P(\Gamma^{-1})$. As shown in the bottom figure,[66] $P(\Gamma^{-1})$s are not unique and depends on the sample position (should be written as $P_p(\Gamma^{-1})$), indicating that a gel (branched polymer) is nonergodic.

Figure 10 shows (a) the intensity-time correlation function (ICF) and (b) corresponding $P(\Gamma^{-1})$s of the NIPA branched polymer systems with various C_{NIPA}.[66] It is clear from the figure that relaxation becomes slower by increasing C_{NIPA} up to $C_{\mathrm{NIPA}} \approx 100$ mM, and then faster for $C_{\mathrm{NIPA}} > 100$ mM. At $C_{\mathrm{NIPA}} \approx 100$ mM, ICF exhibits a power-law behavior given by Eq. 26. At the same time, the intercept of ICF at $t = 0$, i.e., σ_{I}^2, starts to deviate from unity. This is an indication of the appearance of nonergodicity. In Fig. 10b, the characteristic broadening is clearly observed for $C_{\mathrm{NIPA}} = 88$ and 100 mM. Note that this broadening ranges over 5 orders of magnitude of Γ^{-1} in this particular case. $P(\Gamma^{-1})$ indicates that the cluster size becomes huge compared to the individual size of polymer chains formed without cross-links. This figure clearly indicates that a gelation threshold can be determined as a power-law behavior in ICF or as a characteristic broadening of $P(\Gamma^{-1})$.

This observation can readily be applied to construct a sol–gel phase diagram for NIPA/BIS systems. We prepared various NIPA gels with various values of (C_{NIPA}, C_{BIS}) while their ratio ($R_{\mathrm{BIS}} \equiv 2C_{\mathrm{BIS}}/(C_{\mathrm{NIPA}} + 2C_{\mathrm{BIS}})$) were constant and we pursued sets of (C_{NIPA}, C_{BIS}) at which a power-law behavior appeared.[67] The result is shown in Fig. 11. The open circles with dotted lines and filled circles indicate the sets of (C_{NIPA}, C_{BIS}) investigated and the set at which ICF exhibits a power-law. The solid squares indicate sets of (C_{NIPA}, C_{BIS}) at which the system was opaque (i.e., phase separated). Note that this figure reminds one of the site-bond percolation phase diagram (Fig. 1). To our knowledge, this experimental observation is

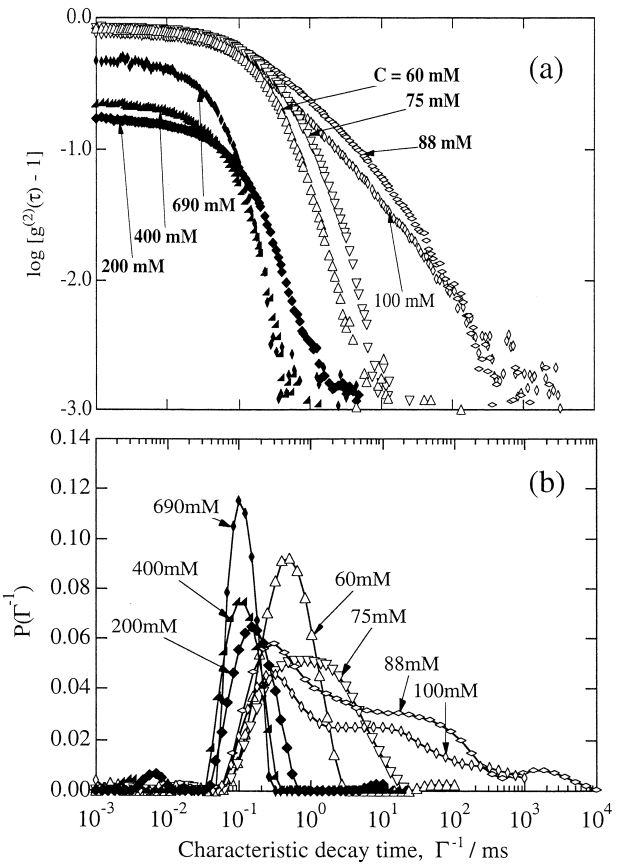

Fig. 10. (a) Intensity correlation function and (b) the distribution function of branched NIPA polymers in water.

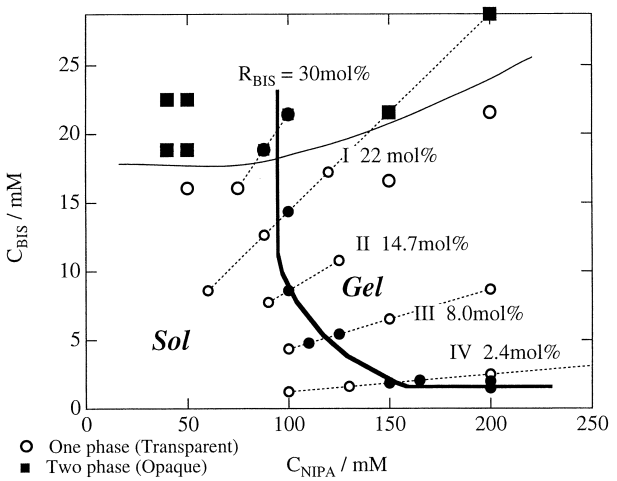

Fig. 11. Sol–gel transition phase diagram for NIPA gels determined by DLS. Open circles, closed circles denote concentrations (C_{NIPA}, C_{BIS}) at observation and those exhibiting a power law behavior in ICF.
[Reproduced with permission from *Macromolecules*, **33**, 2909–2915 (2000). Copyright 2000 Am. Chem. Soc.]

the first piece of evidence for the site-bond percolation model.[11,12]

3. 3. Time-Resolved Dynamic Light Scattering from Gelling Systems and Four Methods of Gel Point Determination. An inorganic gel of silica was chosen for an in situ study of sol–gel transition dynamics by TRDLS.[61] Prescribed amounts of tetramethoxysilane (TMOS) monomer were dissolved in 9 mL of *N*,*N*-dimethylformamide (DMF) in a 10 mm-diameter test tube at room temperature under N_2 purge. The polymerization/gelation of the samples described above was initiated by adding 0.236 mL of 1 N HCl (catalyst). TRDLS measurements were carried out at 58 °C as a function of polymerization time, *t*. The gelation process of this system was rather slow. More than 70 h were required to complete the reaction, which was slow enough for a TRDLS measurement. During the gelation process, the scattering intensity, $I(t)$, and the time correlation function (ICF), $g^{(2)}(t) - 1$, were collected as a function of reaction time; these are displayed in Figs. 12a and b. As shown in Fig. 12a, $<I>_T$ started to increase at 16.69 h. The ICF became flattened with *t* and a power-law behavior appeared exclusively at 16.69 h (No. 4 curve). Both of these phenomena are in accord with those observed in NIPA gels at the critical NIPA concentration. Therefore, it can be deduced that this reaction time corresponds to the gelation threshold, t_{th}. At this time, the cluster distribution function, $G(\Gamma^{-1})$ became widest and the initial amplitude drops suddenly, as shown in Figs. 12c and d, respectively. All of these phenomena indicate the onset of gelation, as discussed above.

On the basis of these findings, we proposed four methods of gel point determination. These methods are different from conventional methods, such as rheological methods or light scattering methods, since the four methods are nondestructive and no dilution is required. Note that each of these methods is a phenomenon based on the characteristic features of gels, i.e., *inhomogeneity* (a), *connectivity divergence* (b, c), and *noner-*

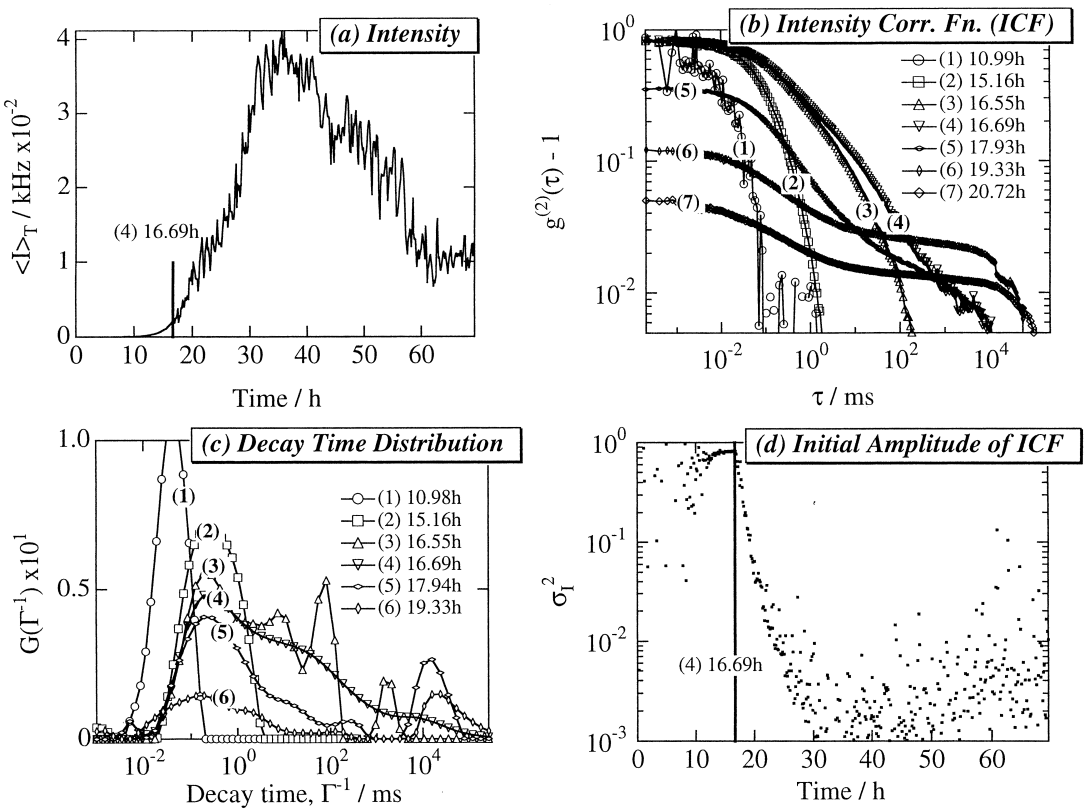

Fig. 12. Four methods to determine the gelation threshold. (a) intensity change, (b) a power-law behavior in ICF, (c) a characteristic broadening of distribution function, and (d) suppression of the initial amplitude of ICF, σ_I^2.

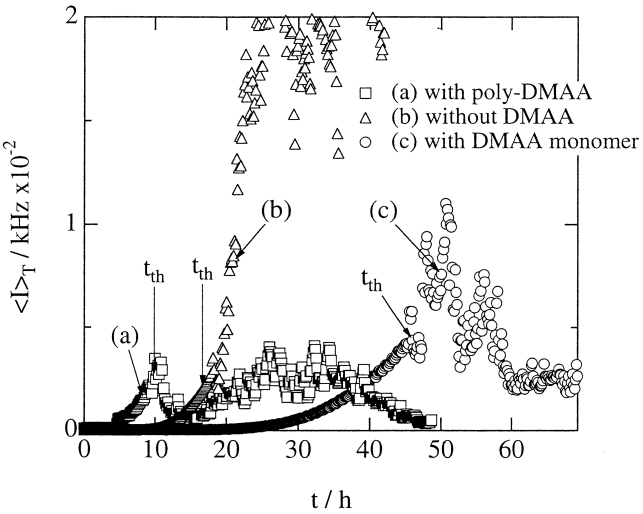

Fig. 13. Scattering intensity variation, $<I(t)>_T$, during polymerization process of TMOS (a) in the presence of poly-DMAA, (b) without DMAA, and (c) presence of DMAA monomer.
[Reproduced with permission from *Macromolecules*, **32**, 1528–1533 (1999). Copyright 1998 Am. Chem. Soc.]

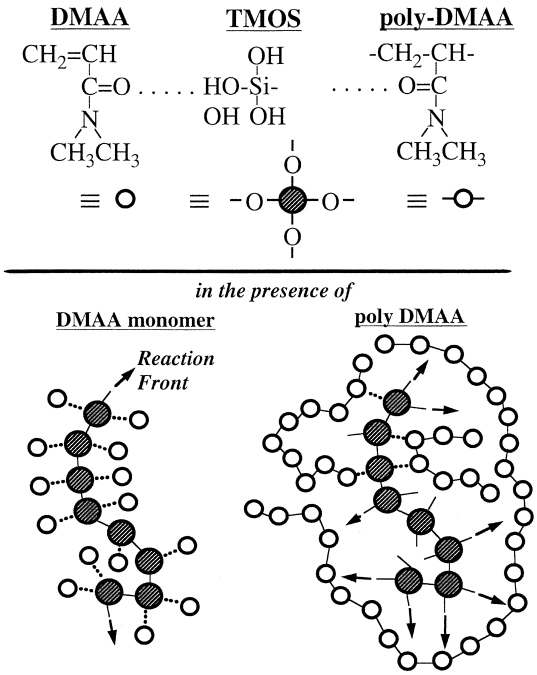

Fig. 14. Possible mechanism explaining the acceleration and deceleration of TMOS polymerization by poly-DMAA and DMAA monomer, respectively.
[Reproduced with permission from *Macromolecules*, **32**, 1528–1533 (1999). Copyright 1999 Am. Chem. Soc.]

godicity (d). These methods are very promising in gelation control for industry. In the following section, the validity and applicability of the four methods will be examined.

4. Chemical Gelling System: Silica Gel

4.1 Organic-Inorganic Polymer Hybird. Organic-inorganic polymer hybrids have recently been synthesized by the so-called sol–gel method of alkoxysilanes.[68,69] The sol-gel reaction comprises hydrolysis and subsequent condensation reaction of alkoxy- or hydroxysilanes to form a Si–O–Si linkage. With further hydrolysis and condensation, a siloxane network develops via cross-linking of the oligomers. Studies on sol-gel reaction of polymer hybrids, however, are intricate due to the following reasons: (1) They are multi-component systems. (2) A complicated chemistry, such as hydrolysis and condensation, is involved. (3) Glassy materials are formed after gelation, which means formation of a nonequilibrated or frozen structure. The four methods introduced above are particularly useful to characterize the gelation kinetics of polymer hybrids.

Here, we discuss the effects of the presence of *N*,*N*-dimethylacrylamide (DMAA) monomer and DMAA (poly-DMAA) polymer in the polymerization/cross-linking reaction of TMOS.[61] Figure 13 shows the intensity variation during polymerization of TMOS (a) in the presence of poly-DMAA, (b) in the absence of DMAA, and (c) in the presence of DMAA monomer. The details of the sample preparation method are described elsewhere.[70] The gelation process of TMOS was found to be strongly dependent on whether or not DMAA polymers/monomers are present in the reaction bath. In the presence of poly-DMAAs (a), the gelation was accelerated, while it was decelerated when DMAA monomer was present in the system (c), with respect to the case of TMOS without any additives (b). Another conclusion which can be drawn from the figure is that the peak intensity around the gelation threshold seems to depend on the architecture of DMAA. When poly-DMAAs exist, the concentration fluctuations of the system are highly suppressed. This is due to the fact that DMAA polymer chains filled in the reaction bath prevent TMOS clusters from evolution of their concentration fluctuations in the free space and allow them to grow in a cage of entangled poly-DMAA chains. These phenomena were also seen in poly(vinyl alcohol) systems.[61]

The effects of DMAA on the gelation of TMOS were deduced as follows. In the presence of DMAA monomer, active reaction sites of TMOS are capped with DMAA monomers by hydrogen bonding between the amide group in DMAA and the silanol group in TMOS (Fig. 14). This interaction is also expected in the TMOS/poly-DMAA system. However, due to the existence of connectivity of the polymer chain, the poly-DMAA chains act rather as guides to coordinate TMOS monomers so as to react with the growing TMOS chains as shown in the figure. This is a kind of "cage effect", which results in an acceleration of the reaction of TMOS/poly–DMAA system.

4.2. Comparison of Silica Gels Prepared with Acid and Base Catalyst. The gelation of TMOS greatly depends on the pH of the catalyst. In order to clarify the gelation mechanism of TMOS, gelation time was studied as a function of the initial monomer (TMOS) concentration, C (3, 4.5, 5, 10 wt%), at fixed catalyst concentrations. Prescribed amounts of TMOS were dissolved in 9 mL of *N*,*N*-dimethylformamide (DMF) in a 10 mm diameter test tube at room temperature under N_2 purge. Polymerization/gelation of TMOS was initiated by adding 0.24 mL of 0.1 N HCl (acidic catalyst) or 0.28 mL of 2.9 N NH_3 aqueous solution (basic catalyst) just before TRDLS measurements. Figure 15 shows the double logarithmic plots of ICFs

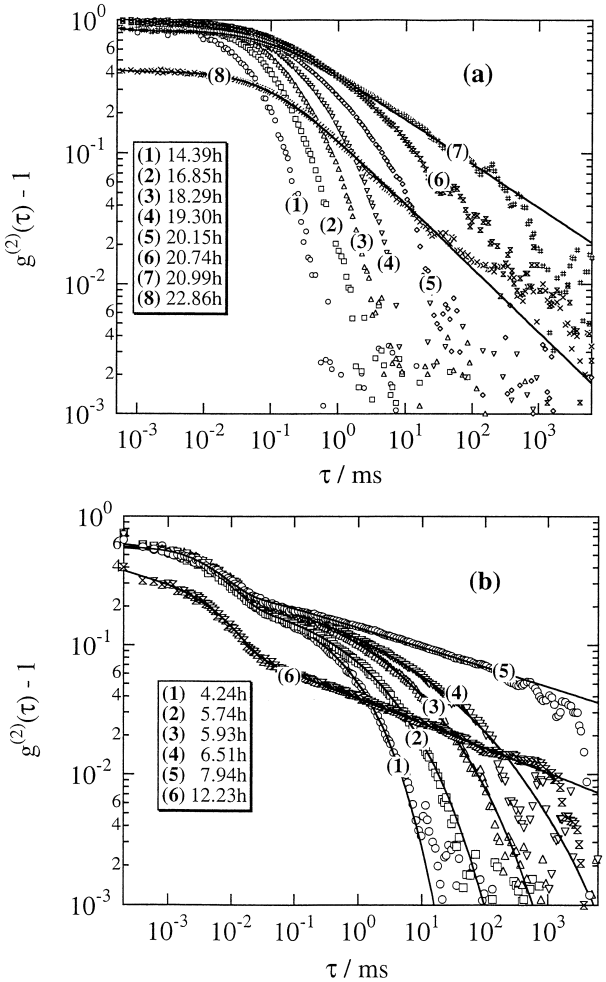

Fig. 15. Changes of ICF during polymerization process of TMOS in (a) acidic and (b) basic conditions.
[Reproduced with permission from *Macromolecules*, **33**, 900–905 (2000). Copyright 2000 Am. Chem. Soc.]

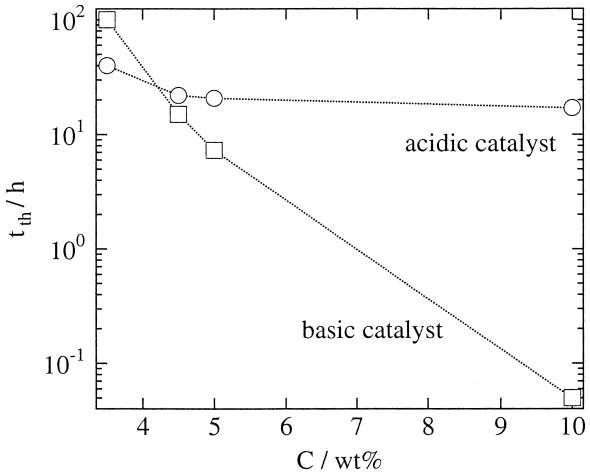

Fig. 16. Concentration dependence of gelation threshold time, t_{th}, for TMOS prepared in acidic and basic conditions.
[Reproduced with permission from *Macromolecules*, **33**, 900–905 (2000). Copyright 2000 Am. Chem. Soc.]

during gelation process for (a) the acidic and (b) the basic systems ($C = 5$ wt%). In the case of the acidic system, the scattered photons are too few to build ICF in the beginning ($t < 14$ h). However, for $t > 14$ h, ICF shows a characteristic decay time at $\tau \approx 10^{-1}$ ms. At $\tau \approx 21$ h, the ICF has a long tail at the larger value of τ. At this point, the ICF seems to be well described with a power law function, indicating $t_{th} \approx 21$ h. The solid lines on the curves (7) and (8) in Fig. 15a were obtained by fitting ICF with Eq. 26 to the case of $t = 20.99$ and $t = 22.86$ h. This fit gives $n = 0.60 \pm 0.04$. The value, however, decreases to 0.5 with time ($t > t_{th}$). For $t > 20.99$ h, the value of $\sigma_I^2 \equiv [g^{(2)}(\tau \to 0) - 1]$ becomes much lower than unity due to the nonergodicity of the gel. As shown in Fig. 15b, the shapes of the ICFs for the basic system, however, are different from those of the acidic system. The values of n are larger than 0.7. This suggests that the gel is highly branched. The solid lines are the fits with Eq. 25 (i.e., a stretched exponential function), which reproduce ICFs quite successfully.

Figure 16 shows the variation of t_{th} with C for (a) acidic and (b) basic systems. The gelation time for the acidic system gradually decreases with increasing C. However, t_{th} is rather C independent and is estimated to be roughly 20 h. This may be due to slow kinetics of hydrolysis (electrophilic reaction) and subsequent condensation.[71] On the other hand, t_{th} for the basic system strongly depends on C, and t_{th} varies from hundreds of hours to a few seconds by changing C from 2% to 10%. Though this type of strong pH dependence in gelation kinetics was also reported by Yamane et al.,[71] such a strong C dependence of t_{th} was disclosed in this TRDLS experiment.[62]

In Fig. 17a is shown a growth of silica clusters prepared with an acidic catalyst. Because propagation of a linear chain is dominant compared with branching, the reaction is similar to a polymerization of linear polymer chains with a small fraction of cross-links. In this case, the excluded volume effect is strongly screened by neighboring chains. This leads to $n \approx 0.5$ as observed by Winter et al.[21] A basic catalyst, on the other hand, makes a TMOS monomer to be a tetrafunctional silanol group, leading to a highly branched cluster formation. In this case, n is expected to be 3/4. As a matter of fact, the TRDLS measurements gave $n \approx 0.73$ in our study. Therefore, the growth of silica clusters seems to be as drawn in Fig. 17b. The findings disclosed in this work are in good agreement with the review by Brinker and Scherer,[72] who discussed the structure of silica gels on the basis of experimental results obtained by viscosity and small-angle X-ray scattering measurements. That is, an acid catalyst leads to chain-like (or linear) molecules, while highly branched clusters are formed by basic catalyst.

5. Sol–Gel Transition in Physical Gels

As discussed in Sec. 1, scattering from gels originates from the spatial inhomogeneities and thermal concentration fluctuations. It has generally been believed that the spatial inhomogeneities are characteristic features of chemical gels because spatial inhomogeneities are instantaneously introduced during polymerization and/or cross-linking processes. Due to the thermoreversible nature of physical gels, on the other hand, it has been thought that spatial inhomogeneities can be easily erased

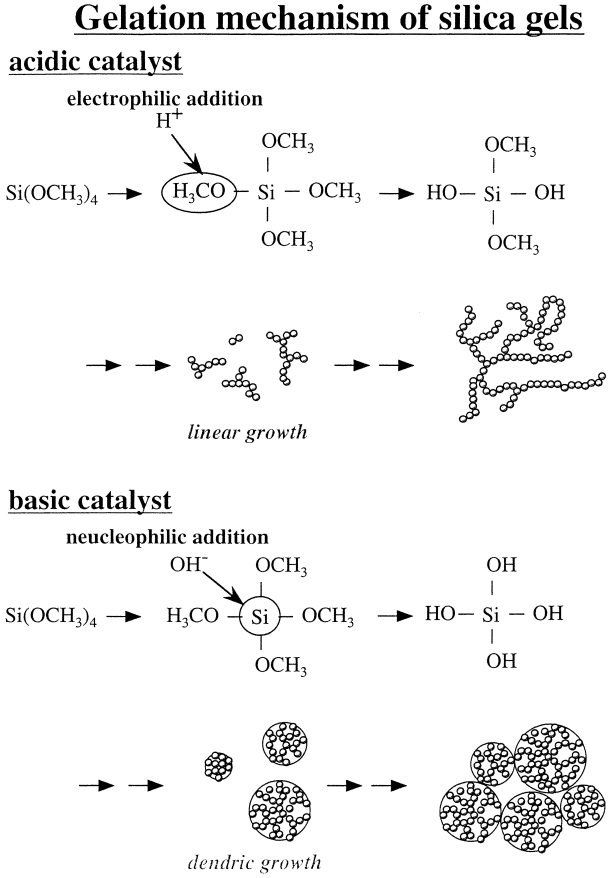

Fig. 17. Schematic models showing growing process of silica clusters in acidic (upper) and basic (lower) conditions.

by dissolving the gel. In this section, it will be proved that this hypothesis is incorrect and a sol–gel transition can be analyzed in the same manner as in the case of chemical gels, such as by speckles in scattering intensity and power law behavior in ICF, as discussed in the previous sections. Furthermore, comparison between temperature-induced and concentration-induced sol-gel transition will be made in connection with site-bond percolation theory.

5.1. Poly(vinyl alcohol)–Congo Red Complex Gels. The first observation of thermoreversible speckle appearance/annihilation in physical gels was made on poly(vinyl alcohol)/Congo Red complex gels (PVA/CR). Poly(vinyl alcohol)/Congo Red (PVA/CR) gels in aqueous solutions were chosen because of the following reasons: (1) the system is transparent though it is colored red, (2) the gelation is governed by chemical equilibrium and hence the rate is quick enough (a few minutes) without hysteresis, (3) the sol–gel transition temperature, T_{gel}, is located at a temperature of easy handling, i.e., ~43 °C, and (4) the sol–gel phase diagram,[73] the microscopic structure,[74] and (4) its enthalpy of gel melting were well characterized.

5.1.1. Sol–Gel Transition. An aqueous solution of reagent grade Congo Red (CR; $C_{32}H_{22}N_6Na_2O_6S_2$), a synthetic dye, was mixed with a PVA solution. The degree of polymerization and degree of saponification of the PVA was 1800 and 99.96 mol%, respectively. CR acts as a cross-linker of PVA via hydrogen bonding between $-NH_2$ group of CR and –OH group of PVA.[75] The sol–gel transition temperature was determined to

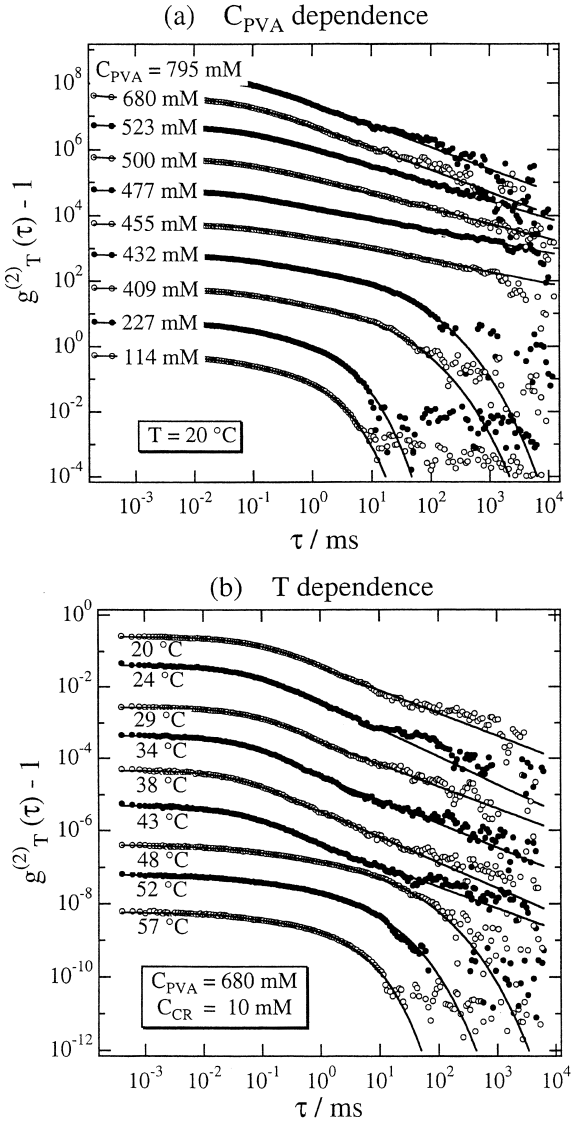

Fig. 18. Time intensity correlation function, $g_T^{(2)}(\tau)$, for PVA/CR aqueous systems (a) at different C_{PVA}'s and (b) at different temperatures, T. In order to avoid overlap, $g_T^{(2)}(\tau)$'s are shifted vertically with a step of one as C_{PVA} or T increases. The solid lines are the results of curve fitting with a stretched exponential function (Eq. 25) and with a power law function (Eq. 26).
[Reproduced with permission from *Macromolecules*, **33**, 7868–7876 (2000). Copyright 2000 Am. Chem. Soc.]

be $T_{gel} \approx 43$ °C by tilting-a-tube method. The details of the experiment and the sol–gel phase diagram are reported elsewhere.[73]

Figures 18a and b show a series of ICFs obtained for PVA/CR (a) at different PVA concentrations, C_{PVA}, and (b) at different temperatures. The sol–gel transition is clearly suggested by the change of the shape of ICF (a) at $C_{PVA} \approx 455$ mM and (b) between 43 and 48 °C. Hence, it is clear that the PVA/CR systems undergo a concentration- or temperature-induced sol–gel transition. For $T < 43$ °C or $C_{PVA} > 455$ mM, the ICF's are well represented by the power-law function (Eq. 26). On the other hand, the functional form of the ICF suddenly changes to

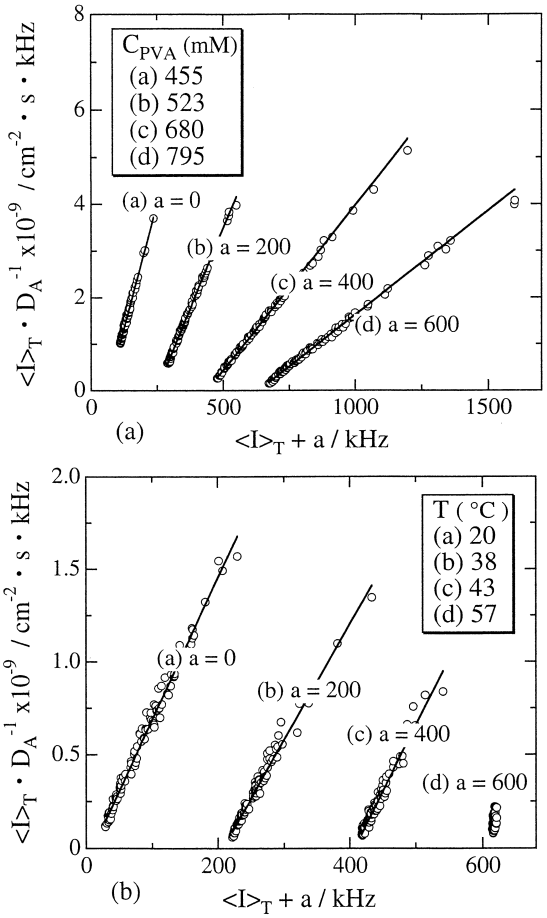

Fig. 19. Decomposition plot for (a) PVA/CR with various C_{PVA}'s at T = 20 °C and for (b) PVA/CR with various T's. The symbol a is a horizontal shift factor introduced to avoid overlap. The solid lines are the fits with Eq. 26. [Reproduced with permission from *Macromolecules*, **33**, 7868–7876 (2000). Copyright 2000 Am. Chem. Soc.]

a stretched exponential function for $C_{PVA} \leq 432$ mM and for $T > 48$ °C. These results clearly indicate that the dynamics changes drastically at the sol–gel transition temperature or at the sol–gel transition concentration. It should be noted that speckles appeared exclusively in the same region where the power law was observed.

The fast mode, i.e., the so-called gel mode, was analyzed via Eq. 16. The results are plotted in Fig. 19, where a is a horizontal shift factor introduced to avoid overlap.[76] The solid lines are the fits with Eq. 16. It is clear from the plots that the slope of the fit decreases with increasing C_{PVA}. This indicates that D (the inverse of the slope) increases significantly with increasing C_{PVA}. Surprisingly, such a notable change is not observed when temperature is scanned. When a gel melts and becomes a sol (i.e., an ergodic medium) at T = 57 °C, all data points collapse at a single point $D_A = D$ in the plot of $<I>_T/D_A$ vs $<I>_T$. The following should be noted. The values of D evaluated at scattering angles of 40–140 ° were identical within the experimental error, suggesting that the fast mode is diffusive.

5.1.2. Sol–Gel Transition vs Site-Bond Percolation. The collective diffusion coefficient was then converted to the correlation length, ξ, with Eq. 19, and values are plotted in Fig. 20. The top-left part of Fig. 20 illustrates a phase diagram based on the site-bond percolation proposed by Coniglio et al.[11] The ordinate and abscissa denote the bond probability and site probability, which correspond to the cross-link concentration and polymer concentration, respectively. Since the cross-link concentration decreases with increasing T, an increase in the bond probability means a decrease in T. These figures clearly show that the site percolation is different from the bond percolation. A continuous variation of ξ is observed in the case of the temperature-induced sol-gel transition and no anomaly is observed at T_{gel}, as shown in (A). On the other hand, a cusp-like transition in ξ is involved in the concentration-induced sol–gel transition (B), which is due to the cross-over of the so-called chain overlap concentration. The correlation length becomes largest at this concentration and the system undergoes a connectivity transition from unpercolated to percolated clusters. In the case of the temperature-induced sol–gel transition, the transition is simply manifested by a switching on and off of cross-links. Hence, the correlation length varies smoothly across the sol–gel transition temperature. This is why no characteristic change in the temperature-induced sol–gel transition has been observed in thermoreversible polymer gels. We believe that the results disclosed here provide an important aspect of the sol–gel transition and the nature of connectivity transition.

The reasons for the difference in the variations of ξ disclosed above can be explained with schematic illustrations in Fig. 21. In the concentration regime of $C_{PVA} < C_{PVA,\,gel}$ (i), the PVA chains do not percolate yet, and form "microgels". In this regime, translational diffusion of microgel clusters is observed by DLS. Therefore, ξ increases with C_{PVA} ($< C_{PVA,\,gel}$) until the clusters fill the space (ii). The following decrease in ξ for $C_{PVA} > C_{PVA,\,gel}$ corresponds to a decrease in blob size by further increase in C_{PVA} (iii–iv). In contrast to the concentration-induced sol–gel transition, the temperature-induced sol–gel transition is governed by chemical equilibrium of complexation of CR with PVA. In Fig. 21b, active CR molecules participating in cross-linking are shown with filled circles, while free CR molecules are denoted by open circles. As shown in the figures, a lowering in temperature (i to iv) results in activation of cross-link formation. Therefore, the mesh size becomes smaller by decreasing T. In this process, no anomaly is expected in the spatial correlation, while the connectivity correlation may diverge at the sol–gel transition.[77] This is what happens in the temperature-induced sol–gel transition. Hence, a monotonous decrease in ξ is observed by decreasing T without divergence in ξ at T_{gel}.

5.1.3. Reentrant Sol–Gel Transition. PVA/CR aqueous solutions exhibit an interesting reentrant sol–gel transition behavior. This is due to the fact that PVA becomes a polyelectrolyte by complexing with CR ion, resulting in a shift of C^* to a lower PVA concentration. However, this shift disappears soon or later by further addition of CR since added CR ions screen the electrostatic interaction between charged PVA chains. Hence, a reentrant behavior in speckles and power-law behavior was anticipated as an additional proof of the gel point determination methods as discussed in this article. DLS measurement on PVA/CR with $C_{PVA} \approx C^*$ was carried out as a function of C_{CR}. As expected, a reentrant appearance/annihila-

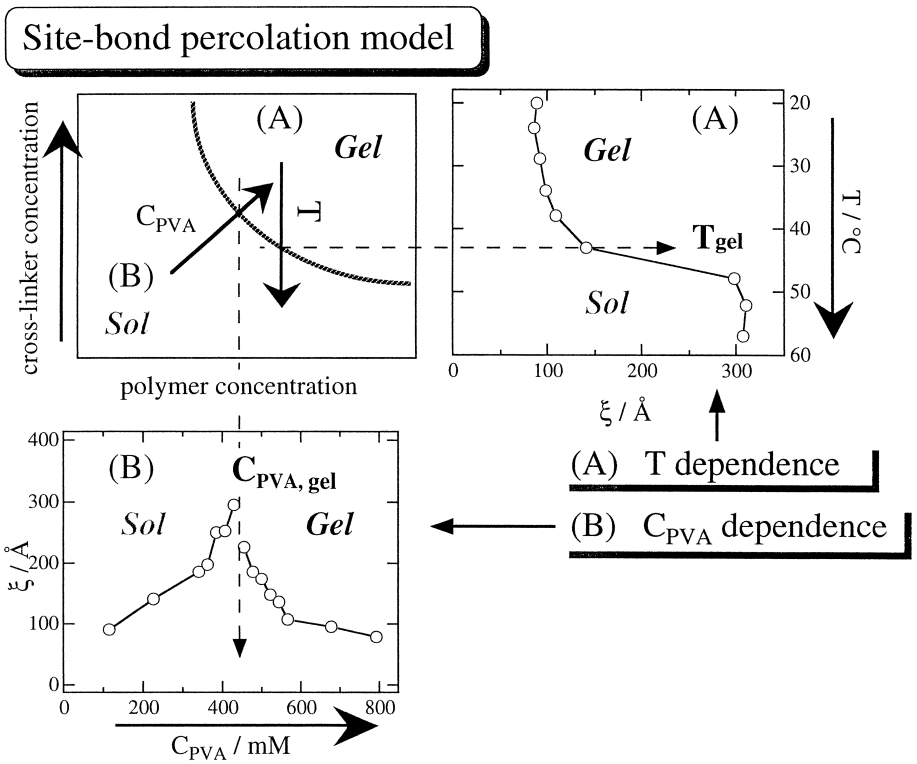

Fig. 20. Schematic representation of the site-bond percolation phase diagram, which explains the (A) temperature and (B) C_{PVA} dependence of ξ. [Reproduced with permission from *Macromolecules*, **33**, 7868–7876 (2000). Copyright 2000 Am. Chem. Soc.]

tion of speckles and power-law-to stretched exponential transition was observed.[78]

5.2. Gelatin. A large number of studies on gelation of gelatin have been carried out from the viewpoints of rheology,[79–83] structure,[84] and optical rotation.[85] However, compared to the understanding on chemical gels, many problems still remain unsolved for gelatin gels. This is partially due to complexity of the chemical structure of gelatin which depends on preparation methods, and uncertainty of cross-linking mechanism, and hysteresis of gelation and gel-melting. Gelatin itself is usually a mixture of α (single helix), β (double helix), and γ (triple helix) gelatin.[16]

Here, we demonstrate two cases of sol–gel transition of gelatin aqueous solutions, i.e., constant cooling/heating process and gelatin gels aged after temperature jump. Since gelation kinetics of natural gel greatly depends on the source and the way of purification, we paid special attention to the choice of gelatin. Alkali-treated Gelatin, extracted from calf bone (photographic grade type, P-3201; $<M>_w = 1.45\times10^5$), kindly supplied by Nitta Gelatin Co., Osaka, Japan, was chosen since it had quite similar molecular characteristics to the gelatin studied by Djabourov et al.[25] The isoelectric point for the sample is pH 4.97. The weight average molecular weight is 1.45×10^5 as determined by gel permeation chromatography. The gelatin was immersed in distilled water for 10 min, followed by dissolution at 50 °C for 1 h. In order to avoid biological contamination, 400 ppm of sodium azide (NaN_3) was added to the gelatin solution. The pHs of the gelatin solutions were around 6.5 irrespective of concentration. After filtration with a 0.45 μm-micropore filter, the gelatin solution was poured in an 8 mm-test tube.

Figure 22 shows temperature variation (top), the time evolution of the time-average scattered intensity, $<I>_T$ (center), and the initial amplitude of ICF, σ_I^2 (bottom), of a 2.5 wt%-gelatin solution during cooling process (left) from 50 to 10 °C and heating process (right) from 10 to 50 °C.[86] The scattering angle was 90°. At the beginning, $<I>_T$ remained constant up to t = 250 min, but started to increase with large fluctuations at $t >$ 300 min (T = 22 °C). These fluctuations and the increase in $<I>_T$ are ascribed to an emergence of nonergodicity as the system becomes a gel. As with the gelation process, gel-melting behavior can be monitored by $<I>_T$ and σ_I^2, as shown in the right figure, where strong fluctuations are suddenly suppressed at t = 220 min (T = 30 °C). Similarly to the cases of chemical gels (Fig. 10), silica gels (Figs. 12, 15), and PVA gels (Fig. 18), a characteristic power law behavior was observed exclusively at the gelation threshold.

Figure 23 shows ICFs of gelatin aqueous systems rapidly quenched to 10 °C and aged for 20 days.[87] The gelatin concentrations, C, were in the range of $0.05 \leq C \leq 15$ wt%. For the gelatin samples with low concentrations ($C \leq 0.20$ wt%), a single decay was observed; the relaxation became slower with increasing C. When C reached 0.35 wt%, a power-law type behavior was observed in the ICF as depicted with the solid line. The power-law behavior in an ICF is recognized to be a characteristic of gelation threshold as discussed above. Hence, the lowest sol-gel transition concentration seems to be $C_{gel} \approx$ 0.35 wt%. By further increasing C, one finds that the initial amplitude of ICF deviates from unity as a result of emergence of nonergodicity (i.e., appearance of speckles), which is again

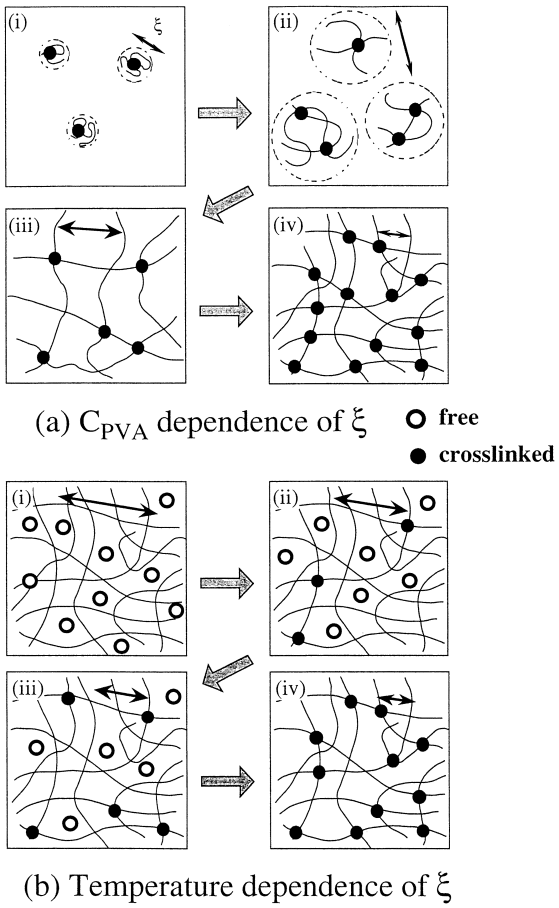

Fig. 21. Illustrations explaining (a) the C_{PVA} and (b) T dependence of ξ. C_{PVA} increases but T decreases from (i) to (iv). Open and filled circles denote free and cross-linked CR molecules. The arrows in the figures indiate the length of ξ. [Reproduced with permission from *Macromolecules*, **33**, 7868–7876 (2000). Copyright 2000 Am. Chem. Soc.]

another indication of gel state. The value of exponent n was estimated to be around 0.4, which is significantly lower than the one obtained for a quenched gelatin gel (C = 2.5 wt%) undergoing gelation ($n \approx 0.7$).[86] A gelatin gel prepared from its lowest gelation concentration, i.e., $C_{gel} \approx 0.35$ wt%, seemed to be less branched. In other words, it has a similar structure to that of a silica gel prepared with an acidic catalyst (Fig. 17a).

6. Other Systems

6.1. Protein Gelation by Heating.[88] Heat-induced gelation of β-lactoglobulin (β-LG) in aqueous solutions at pH 2 and 7 was investigated by TRDLS. Similar results to the gelation process of TMOS were obtained, i.e., appearance of speckle and a power-law behavior in ICF at the gelation threshold, t_{th}. The exponent n was found to be strongly dependent on pH. The values of n were 0.51 ± 0.05 for pH 2 and 0.74 ± 0.05 for pH 7. These findings indicate that β-LG gels formed at pH 2 and pH 7 have different architectures, i.e., loosely tied networks (for pH 2) and fractal aggregates (for pH 7) of protein molecules, which is again similar to the case of silica gels discussed in Sec. 5.2.

6.2. Bulk Polymerization of Polystyrene and Poly(styrene-*co*-divinylbenzene). Ren and Sorensen demonstrated that gelation of gelatin was analogous to the α- and β-relaxation of a glass-forming liquid.[89,90] However, the analogy between these two interesting phenomena, i.e., gelation and vitrification, has not been extensively discussed in the literature, even though both can be described by percolation theory.[91] A topological difference between gelation and vitrification may be found in the chain connectivity. If the power-law in ICF

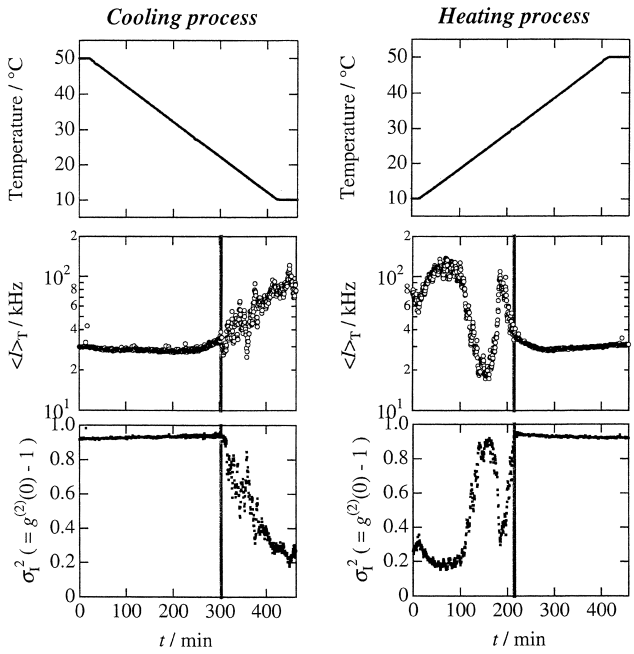

Fig. 22. Variation of sample temperature (top), the scattered intensity, $<I>_T$, and initial amplitude of ICF, σ_I^2 (bottom) with time, t, for a gelatin gel with 2.5 wt% during cooling process from 50 to 10 °C (left) and heating process (right) with the rate of 0.10 °C/min. The shaded line indicates the sol-gel transition threshold.

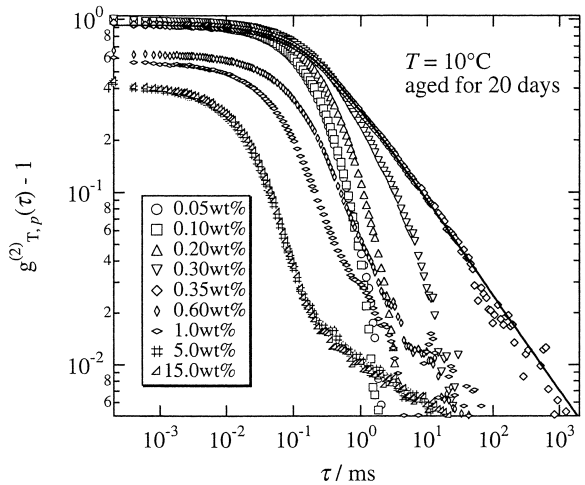

Fig. 23. Time-intensity correlation functions (ICF), $g^{(2)}{}_{T,p}(\tau)-1$, for gelatin solutions and gels with various concentrations at T = 10 °C.
[Reproduced with permission from *J. Chem. Phys.*, **115**, 4285–4291 (2001). Copyright 2001 Am. Inst. Phys.]

originates from connectivity divergence characteristic of gelation, experimental comparison of vitrification process with gelation process is of much interest. In order to examine the relation between connectivity divergence and power-law behavior, the TRDLS method was applied to study bulk-polymerization process of polystyrene[92] and the difference of polymer chain dynamics during polymerization process of linear (polystyrene; PSt) and branched polymer chains (a mixture of St and polydivinylbenzene; DVB) was compared. In both systems, the polymerization temperature was 60 °C, which is much lower than the glass transition temperature of PSt ($\approx$ 100 °C). Therefore, it was expected that the reacting systems vitrified during the polymerization process.

As was conjectured, the ICF of the St–DVB mixture exhibited a power law behavior exclusively at the gelation threshold. On the other hand, polymerization of St at 60 °C resulted in formation of vitrified linear polystyrene without showing a power law behavior in ICF. Therefore, it was concluded that the TRDLS was able to detect the gelation threshold even for bulk polymerization of St–DVB and to discriminate gelation from vitrification by polymerization.

7. Concluding Remarks

Nondestrictive in-situ DLS methods for gelation threshold determination were proposed and their validity as well as applicability was examined. The gelation threshold was characterized by an appearance of (1) speckle patterns in scattering intensity and (2) a power-law behavior in intensity time correlation function (ICF), (3) a specific broadening of distribution function, $G(\Gamma)$, and (4) a noticeable suppression of the initial amplitude of ICF. These characteristic behaviors indicating gelation are due to inhomogeneities, nonergodicity, and connectivity divergence at the gelation threshold. The universality of these phenomena was examined in various types of gelling systems, such as organic chemically gelling systems (NIPA gels and polyacrlyamide gels), inorganic gels (TMOS), polymer hybrid (TMOS/DMAA), polymer-ion complexes (PVA/Congo Red) undergoing reversible sol-gel transition, natural polymers (gelatin and β-lactoglobulin), and bulk polymerization of styrene and divinylbenzene mixtures. In all systems, the four characteristic signals ((1)–(4)) were exclusively observed at the gelation threshold. Therefore, it can be concluded that the four methods proposed above can be used to determine the gelation threshold.

Besides gel point determination, it was demonstrated that TRDLS is a powerful tool to investigate molecular dynamics of gelling (or cross-linking) systems near the gelation threshold. Particularly, the critical dynamics is uniquely described by a power-law function in ICF, indicating a self-similar nature of clusters near gelation threshold. It is concluded that the sol–gel transition of both chemical and physical gels is well described by the site-bond percolation theory.

The power-law exponent was found to be dependent on the architecture of the gelling system though its physical implementation needs further theoretical investigation. The value of n was found to increase with increasing degree of branching of gelling clusters.

Most of the works described in this article were carried out at the Department of Polymer Science and Engineering, Kyoto Institute of Technology, during the period of 1994 to 2000. This work was partially supported by the Ministry of Education, Science, Sports and Culture (Grants-in-Aid, 12450388 and 13031019). Financial support was also made by Cosmetology Foundation (Tokyo) and Yamada Science Foundation (Osaka).

References

1 "Gel Handbook," ed by Y. Osada and K. Kajiwara Academic Press, New York, (2001).
2 B. J. Eldridge and J. D. Ferry, *J. Phys. Chem.*, **58**, 992 (1954)
3 P. J. Flory, *J. Am. Chem. Soc.*, **63**, 3038 (1941)
4 P. J. Flory, *Chem. Revs.*, **39**, 137 (1946)
5 P. J. Flory, "Principles in Polymer Chemistry," Cornell Univ., Ithaca (1953).
6 W. H. Stockmayer, *J. Chem. Phys.*, **11**, 45 (1943)
7 W. J. Stockmayer, *J. Chem. Phys.*, **12**, 125 (1944)
8 D. Stauffer, *Phys. Rep.*, **54**, 1 (1979)
9 D. Stauffer, A. Coniglio, and M. Adam, *Adv. Polym. Sci.*, **44**, 103 (1982)
10 D. Stauffer, "Introduction to Percolation Theory," Taylor & Francis, London (1985).
11 A. Coniglio and H. E. Stanley, *Phys. Rev. Lett.*, **42**, 518 (1979)
12 A. Coniglio, H. E. Stanley, and W. Klein, *Phys. Rev. B*, **25**, 6805 (1982)
13 J. M. Guenet, "Thermoreversible Gelation of Polymers and Biopolymers," Academic Press, NY (1992).
14 M. Adam and D. Lairez, in "Physical Properties of Polymeric Gels," ed by J. P. Cohen Addad John Wiley & Sons, New York (1996), pp. 87.
15 H. H. Winter and M. Mours, *Adv. Polym. Sci.*, **134**, 167 (1997)
16 K. te Nijenhuis, *Adv. Polym. Sci.*, **130**, 1 (1997)
17 H. G. Shild, *Prog. Polym. Sci.*, **17**, 163 (1992)
18 S. Takata, T. Norisuye, and M. Shibayama, *Macromolecules*, **32**, 3989 (1999)
19 M. Shibayama, H. Yoshizawa, H. Kurokawa, H. Fujiwara, and S. Nomura, *Polymer*, **29**, 2066 (1988)
20 F. Chambon and H. H. Winter, *Polym. Bull.*, **13**, 499 (1985)
21 H. H. Winter and F. Chambon, *J. Rheology*, **30**, 367 (1986)
22 F. Chambon, Z. S. Petrovic, W. J. MacKnight, and H. H. Winter, *Macromolecules*, **19**, 2146 (1986)
23 J.-E. Guenet and G. B. McKenna, *Macromolecules*, **21**, 1752 (1988)
24 M. Kobayashi, A. I., T. Ishii, and S. Amiya, *Macromolecules*, **28**, 6677 (1995)
25 M. Djabourov, J. Leblond, and P. Papon, *J. Phys. Fr.*, **49**, 319 (1988)
26 W. Schmidt and W. Burchard, *Macromolecules*, **14**, 370 (1981)
27 M. Adam, M. Delsanti, J. P. Munch, and D. Durand, *J. Phys.*, **48**, 1809 (1987)
28 J. E. Martin and J. P. Wilconxon, *Phys. Rev. A*, **39**, 352 (1989)
29 E. Bouchaud, M. Delsanti, M. Adam, M. Daoud, and D. Durand, *J. Phys.*, **47**, 1273 (1986)
30 S. Kobayashi, *Rev. Sci. Instrum.*, **56**, 160 (1985)

31 J. C. Dainty, "Laser Speckle and Related Phenomena," Springer-Verlag, Berlin (1975).
32 C. Allain, M. Drifford, and B. Gauthier-Manuel, *Polymer*, **27**, 177 (1986)
33 C. Wu, J. Zuo and B. Chu, *Macromolecules*, **22**, 838 (1989)
34 P. Debye, *J. Phys. Colloid Chem.*, **51**, 18 (1947)
35 B. Zimm, *J. Chem. Phys.*, **16**, 1093 (1948)
36 P. G. de Gennes, "Scaling Concepts in Polymer Physics," Cornell University, Ithaca (1979).
37 M. Shibayama, K. Kawakubo, F. Ikkai, and M. Imai, *Macromolecules*, **31**, 2586 (1998)
38 J. Bastide and S. J. Candau, in "Physical Properties of Polymeric Gels," edited by J. P. Cohen Addad John Wiley & Sons, New York (1996).
39 M. Shibayama, *Macromol. Chem. Phys.*, **199**, 1 (1998)
40 E. Geissler, in "Dynamic Light Scattering, the Methods and Applications," ed by W. Brown Oxford Univ., Oxford (1993).
41 W. Prins, L. Rimai, and A. F. Chompff, *Macromolecules*, **5**, 104 (1972)
42 T. Tanaka, L. O. Hocker, and G. B. Benedek, *J. Chem. Phys.*, **59**, 5151 (1973)
43 T. Tanaka, in "Dynamic Light Scattering," edited by R. Pecora Plenum, NY (1985).
44 E. Geissler and A. M. Hecht, *J. Chem. Phys.*, **65**, 103 (1976)
45 E. Geissler and A. M. Hecht, *J. Phys. (Les Ulis, Fr.)*, **39**, 955 (1978)
46 P. N. Pusey and W. van Megen, *Physica A*, **157**, 705 (1989)
47 J. Z. Xue, D. J. Pine, S. T. Milner, X. L. Wu, and P. M. Chaikin, *Phys. Rev. A*, **46**, 6550 (1992)
48 M. Shibayama, T. Norisuye, and S. Nomura, *Macromolecules*, **29**, 8746 (1996)
49 J. G. H. Joosten, J. L. McCarthy, and P. N. Pusey, *Macromolecules*, **24**, 6690 (1991)
50 B. Chu, "Laser Light Scattering," 2nd ed, ed Academic Press, New York (1991).
51 M. Shibayama, Y. Fujikawa, and S. Nomura, *Macromolecules*, **29**, 6535 (1996)
52 T. Tanaka, in "Dynamic Light Scattering," ed by R. Pecora Plenum Publishing, New York (1985), pp. 347–362.
53 S. W. Provencher, *Comp. Phys. Comm.*, **27**, 213 (1982)
54 S. W. Provencher, *Comp. Phys. Comm.*, **27**, 229 (1982)
55 J. E. Martin, J. Wilcoxon, and J. Odinek, *Phys. Rev. A*, **43**, 858 (1991)
56 M. Antonietti, K. J. Foelsch, H. Sillescu, and T. Pakula, *Macromolecules*, **22**, 2812 (1989)
57 J. E. Martin and J. Wilcoxon, *Phys. Rev. Lett.*, **61**, 373 (1988)
58 D. Durand, M. Delsanti, M. Adam and J. M. Luck, *Europhys. Lett.*, **3**, 297 (1987)
59 M. Muthukumar, *Macromolecules*, **22**, 4656 (1989)
60 M. Doi and A. Onuki, *J. Phys. II Fr.*, **2**, 1631 (1992)
61 T. Norisuye, M. Shibayama, R. Tamaki, and Y. Chujo, *Macromolecules*, **32**, 1528 (1999)
62 T. Norisuye, M. Inoue, M. Shibayama, R. Tamaki, and Y. Chujo, *Macromolecules*, **33**, 500 (2000)
63 T. Norisuye, M. Shibayama, and S. Nomura, *Polymer*, **39**, 2769 (1998)
64 M. Shibayama, Y. Isaka, and Y. Shiwa, *Macromolecules*, **32**, 7086 (1999)
65 H. E. Stanley, "Introduction to Phase Transition and Critical Phenomena," Oxford Univ. Press, New York (1971).
66 T. Norisuye, M. Takeda, and M. Shibayama, *Macromolecules*, **31**, 5316 (1998)
67 M. Takeda, T. Norisuye, and M. Shibayama, *Macromolecules*, **33**, 2909 (2000)
68 B. M. Novak, *Adv. Mater.*, **5**, 422 (1993)
69 U. Schubert, N. Husing, and A. Lorenz, *Chem. Mater.*, **7**, 2010 (1995)
70 R. Tamaki, K. Naka, and Y. Chujo, *Polym. J.*, **30**, 60 (1998)
71 M. Yamane, S. Inoue, and A. Yasumori, *J. Noncryst. Solids*, **63**, 13 (1984)
72 C. J. Brinker and G. W. Scherer, *J. Non-Crystalline Solids*, **70**, 301 (1985)
73 M. Shibayama, F. Ikkai, R. Moriwaki, and S. Nomura, *Macromolecules*, **27**, 1738 (1994)
74 M. Shibayama, F. Ikkai, and S. Nomura, *Macromolecules*, **27**, 6383 (1994)
75 M. Shibayama, in "The Polymeric Materials Encyclopedia: Synthesis, Properties, and Applications," CRC Press, FL (1996), Vol. 9, pp. 7020–7026.
76 M. Shibayama, M. Tsujimoto, and F. Ikkai, *Macromolecules*, **33**, 7868 (2000)
77 T. Freltoft, J. K. Kjems, and S. K. Sinha, *Phys. Rev. B.*, **33**, 269 (1986)
78 M. Tsujimoto and M. Shibayama, *Macromolecules*, **35**, 1342 (2002).
79 G. Cuvelier and B. Launay, *Macromol. Chem., Macromol. Symp.*, **40**, 23 (1990)
80 E. J. Amis, D. F. Hodgson, and Q. Yu, *Polym. Prepr*, **32**, 447 (1991)
81 H. Huang and C. M. Sorensen, *Phys. Rev. E*, **53**, 5075 (1996)
82 J. Peyrelasse, M. Lamarque, J. P. Habas, H. Boedtkaer, and N. E. Bounia, *Phys. Rev. E*, **53**, 6126 (1996)
83 K. te Nijenhuis, *Colloid Polym Sci.*, **259**, 522 (1981)
84 H. Boedtkaer and P. Doty, *J. Phys. Chem.*, **58**, 968 (1954)
85 W. F. Harrington and N. V. Rao, *Biochemistry*, **9**, 3714 (1970)
86 M. Okamoto, T. Norisuye, and M. Shibayama, *Macromolecules*, **34**, 8496 (2001).
87 M. Shibayama and M. Okamoto, *J. Chem. Phys.*, **115**, 4285 (2001)
88 S. Takata, T. Norisuye, N. Tanaka, and M. Shibayama, *Macromolecules*, **33**, 5470 (2000)
89 S. Z. Ren, W. F. Shi, W. B. Zhang, and C. M. Sorensen, *Phys. Rev. A*, **45**, 2416 (1992)
90 S. Z. Ren and C. M. Sorensen, *Phys. Rev. Lett.*, **70**, 1727 (1993)
91 R. Zallen, "Physics of Amorphous Solids," John Wiley & Sons, New York (1983).
92 M. Shibayama, S. Ozeki and T. Norisuye, in "Third Tohwa University International Conference," American Institute of Physics, Fukuoka (1999).

Mitsuhiro Shibayama was born in Nagoya in 1954. He graduated from the Department of Polymer Chemistry, Faculty of Engineering, Kyoto University in 1977. He received a Doctor-of-Engineering degree, from Kyoto University in 1983. After serving as a fellow of the Japan Society for Promotion of Science and as a research associate at the University of Massachusetts at Amherst, he joined Department of Polymer Science, Kyoto Institute of Technology in 1984. He was promoted to an associate professor in 1988 and to professor in 1997. He has been interested in structure investigation with scattering techniques, such as small-angle X-ray and neutron scattering and light scattering on multicomponent systems, such as block copolymers and polymer blends. In 1991, he spent a year at the Physics Department, Massachusetts Institute of Technology, where he was involved in research on volume phase transition of polymer gels. In 2000, he moved to Neutron Scattering Laboratory, Institute for Solid State Physics, the University of Tokyo. His research interest covers structure and dynamics, volume phase transition, and macro- and micro-phase separation of polymer gels, gel inhomogeneities, gelation kinetics, vitrification of glass forming materials, etc. He has received the Sakurada Takeshi Memorial Award (Japan Fiber Society, 1991) and the Wiley Science Award (the Society of Polymer Science, Japan, 2000).

Tomohisa Norisuye was born in Osaka in 1972. He graduated from the Department of Polymer Science, Kyoto Institute of Technology (KIT), in 1995. He received a Doctor-of-Engineering degree from Kyoto Institute of Technology in 1999. During the doctoral course program, he also served as a fellow of Japan society for Promotion of Science in 1999. Since 2000 he has been a research associate at the Department of Polymer Science, Kyoto Institute of Technology. His current research interests cover kinetics of polymeric network formation, protein aggregation, and vitrification using static/dynamic light scattering and small angle neutron scattering techniques.